

1  
2  
3  
4  
5  
6  
7  
8  
9  
10  
11  
12  
13  
14  
15  
16  
17  
18  
19  
20  
21  
22

Convective Distribution of Tropospheric Ozone and Tracers in the Central  
American ITCZ Region: Evidence from Observations During TC4

Author List: Melody Avery, Cynthia Twohy, David McCabe, Joanna Joiner, Kurt  
Severance, Eliot Atlas, Donald Blake, T. P. Bui, John Crouse, Jack Dibb, Glenn  
Diskin, Paul Lawson, Matthew McGill, David Rogers, Glen Sachse, Eric Scheuer,  
Anne M. Thompson, Charles Trepte, Paul Wennberg, Jerald Ziemke

Revised, resubmitted to  
Journal of Geophysical Research, Atmospheres  
TC<sup>4</sup> Special Issue

May 11, 2010

23 Abstract:

24

25 During the Tropical Composition, Clouds and Climate Coupling (TC4) experiment  
26 occurring in July and August of 2007, extensive sampling of active convection in  
27 the ITCZ region near Central America was performed from multiple aircraft and  
28 satellite sensors. As part of a sampling strategy designed to study cloud  
29 processes, the NASA ER-2, WB-57 and DC-8 flew in stacked "racetrack  
30 patterns" in convective cells. On July 24, 2007, the ER-2 and DC-8 probed an  
31 actively developing storm and the DC-8 was hit by lightning. Case studies of this  
32 flight, and of convective outflow on August 5, 2007 reveal a significant anti-  
33 correlation between ozone and condensed cloud water content. With little  
34 variability in the boundary layer and a vertical gradient, low ozone in the upper  
35 troposphere indicates convective transport. Because of the large spatial and  
36 temporal variability in surface CO and other pollutants in this region, low ozone is  
37 a better convective indicator. Lower tropospheric tracers methyl hydrogen  
38 peroxide, total organic bromine and calcium substantiate the ozone results. OMI  
39 measurements of mean upper tropospheric ozone near convection show lower  
40 ozone in convective outflow. A mass balance estimation of the amount of  
41 convective turnover below the tropical tropopause transition layer (TTL) is 50%,  
42 with an altitude of maximum convective outflow located between 10-11 km, 4 km  
43 below the cirrus anvil tops. It appears that convective lofting in this region of the  
44 ITCZ is either a two-stage or a rapid mixing process, because undiluted  
45 boundary layer air is never sampled in the convective outflow.

46

47 1. Introduction:

48

49 **1.1 TC4 mission and goals of this paper**

50 This paper describes observations of trace gas redistribution by convection in the  
51 tropical troposphere, in the vicinity of the inter-tropical convergence zone (ITCZ)  
52 in the Gulf of Panama near Central America. Observational process studies to  
53 characterize vertical tracer transport and associated chemistry in strong tropical  
54 convection are needed to understand carbon and nitrogen budgets, and the  
55 oxidizing capacity of the atmosphere. Although convection is the dominant  
56 process controlling tropical tracer distribution, chemical transport models have  
57 difficulty simulating convective transport and chemistry accurately due to the  
58 dominance of small-scale diabatic processes. It is important to accurately  
59 quantify transport and chemistry of chemical tracers in the tropics because there  
60 is an abundance of energy available for phase transformation and  
61 photochemistry, and there is strong coupling between chemistry, clouds and  
62 climate impacts. Finally, the planetary boundary layer has the most potential for  
63 direct impact on the stratosphere in the tropics.

64

65 The measurements described here were taken from the NASA DC-8, WB-57,  
66 ER-2, balloon sondes and the NASA Aura satellite during the Tropical  
67 Composition, Cloud and Climate Coupling Experiment (TC4), July 17 – August 8  
68 of 2007. TC4 science goals, flight planning and flight summaries are described  
69 in the TC4 overview paper by Toon et. al. [2010]. The TC4 mission included

70 sampling from the DC-8 as a moderate altitude platform, from the WB-57 for  
71 higher altitude sampling in the tropical transition layer (TTL, from 12-17 km) just  
72 below the stratosphere, and highest altitude sampling from the ER-2 with remote  
73 sensors similar to many found on NASA Earth Observing System (EOS)  
74 satellites. Whenever feasible, aircraft flights were planned to be coincident with  
75 an EOS satellite overpass, in order to validate the satellite instrument  
76 observations, or to combine them with the suborbital *in situ* and remote  
77 measurements for analysis.

78

79 The scope of the TC4 mission included measurements to quantify cloud  
80 composition and physics, tropospheric and lower stratospheric composition and  
81 chemistry, and vertical transport by convection. In this paper we focus on  
82 addressing a few of the major TC4 science questions by analyzing data in the  
83 troposphere. These science questions are paraphrased below:

- 84 - "What is the composition of the tropical troposphere below the TTL?"
- 85 - "What are the mechanisms that control ozone within and below the TTL?"
- 86 - "What is the chemical nature of the convective outflow?"

87

## 88 **1.2 Origin of ozone in the upper troposphere**

89 Ozone is important for determining the oxidizing capacity of the atmosphere, and  
90 it is both an infrared and visible wavelength absorber, which either heats or cools  
91 the atmosphere locally, depending on altitude. Processes that control ozone in  
92 the tropical upper troposphere (500-150 hPa) are expected to be predominantly

93 convective outflow from the boundary layer, extra-tropical advection, and *in situ*  
94 photochemical production. The chemical lifetime for ozone loss is about 50 days  
95 in the tropical upper troposphere [Folkins *et al.*, 2006], compared to the typical  
96 vertical mixing time of less than 1 day during TC4 [Pfister *et al.*, 2010], so that  
97 ozone can be used as a dynamical tracer for vertical transport if *in situ* ozone  
98 production is not too large.

99

100 *In situ* ozone production can be enhanced by biomass burning plumes containing  
101 NO<sub>x</sub>, or downwind of electrically active convection by NO produced by lightning  
102 [Pickering *et al.*, 2006]. Direct production of ozone by lightning is difficult to  
103 measure, and apparently rare [Ridley, 2006]. No ozone production was  
104 observed during a lightning strike to the DC-8 during TC4. In the tropics there is  
105 generally plenty of water vapor and sunlight available to form reactive odd  
106 hydrogen-containing radicals (OH+HO<sub>2</sub>≡HO<sub>x</sub>), and carbon monoxide or  
107 hydrocarbons from biomass burning are often available for oxidation and ozone  
108 production. However, ozone is also destroyed very effectively and catalytically  
109 by HO<sub>x</sub> if HO<sub>2</sub> is not efficiently converted to OH by the oxidation and cycling of  
110 NO and NO<sub>2</sub> radicals (NO<sub>x</sub>). In general, ozone formation is NO<sub>x</sub>-limited in the  
111 tropical TC4 study region.

112

113 Tracer sampling of the upper troposphere during TC4 mainly showed well-aged  
114 pollution, well mixed into a clean tropical background. Estimates of the ozone  
115 production rate range between 0.2 parts per billion by volume (ppbv)/hour

116 expected from calculations published by *Folkins et al.* [1999] in the clean tropical  
117 upper troposphere to 0.8 ppbv/hour from the tropical biomass burning case  
118 studied by Pickering et. al. [1996]. Ozone production rates of up to 0.5 ppbv/hour  
119 were calculated during TC4 by Salawitch [plot not shown]. *Morris et al.* [2010]  
120 measured even higher ozone production rates of 1.1-3.2 ppb/hour between 2-5  
121 km in a convective cloud. This suggests that *in situ* ozone production can  
122 sometimes occur vigorously during vertical transport in convection.

123

### 124 **1.3 Meteorology during TC4 and vertical transport**

125 The TC4 study area was chosen to be in the vicinity of the ITCZ so that the  
126 aircraft, balloons and satellite sensors could sample active convection [Toon et.  
127 al. 2010]. During July and August of 2007, Special Sensor Microwave Imager  
128 (SSM/I) rainfall images show that maximum rainfall from the ITCZ was located in  
129 the Gulf of Panama, in the center of the TC4 study area. Sea surface  
130 temperature anomalies in the Eastern Pacific were 1-1.5 degrees below average,  
131 indicating the onset of a moderate cold-phase ENSO event [NOAA Climate  
132 Prediction Center, Diagnostic Discussion]. Comparison with other years showed  
133 less convection and less intense convection during 2007 than usual [*Pfister et al.*,  
134 2010], with stronger than usual easterlies in the upper troposphere that are  
135 typical of the cold phase of ENSO. Examination of the wind measurements  
136 during local sampling in the upper troposphere from the DC-8 using the  
137 Meteorological Measurement System (MMS) [*Scott et al., 1990*] confirms that  
138 >90% of the wind vectors have an easterly component.

139

140 Winds measured in the mid-troposphere during local flights on the DC-8 also  
141 almost always show an easterly component, with a slight bias to the south  
142 compared to the upper tropospheric winds. However, winds at the surface in the  
143 planetary boundary layer are much more complex. Large-scale data analysis  
144 [Pfister *et al.*, 2010] and dust collected from low altitude sampling shows that the  
145 lower level winds brought air from Africa and South America into the boundary  
146 layer in the main TC4 study region, while vector winds measured on the DC-8  
147 show winds coming from all 4 quadrants, and chemical tracers showed a mix of  
148 both polluted continentally-influenced air and very clean maritime air, as  
149 discussed below. While convection in the ITCZ region in 2007 was relatively  
150 weak, analysis by *Hlvaka et. al.* [2010] shows that the TC4 local study area was  
151 still very cloudy, with on average greater than 94% multilayered cloud cover,  
152 most frequently marine stratus decks overlain with cirrus from evolving  
153 convective anvils. Further, periods of active convection were sampled by the  
154 airplanes, particularly at the beginning and at the end of the mission.

155

#### 156 **1.4 Summary**

157 In this paper we look at the impact of these dynamics on the composition of the  
158 upper troposphere in the TC4 study region. First we present an overview of the  
159 distribution and correlations of O<sub>3</sub>, CO and CH<sub>4</sub>, and focus on the composition of  
160 the boundary layer source region. Two case studies are presented during which  
161 the planes sampled active convection and convective outflow. These provide an

162 opportunity to establish whether there are potentially robust tracer correlations in  
163 the extensive DC-8 data set in convectively influenced air. During these two  
164 flights, the inverse relationship between condensed cloud water content (both  
165 water and ice) and ozone is the strongest we found in the fast-response *in situ*  
166 data set, so we test the larger ensemble of upper tropospheric data from the  
167 “racetrack” flights to see if this relationship appears to be true more universally.  
168 Since it does, we use this information to find the altitude of maximum convective  
169 outflow, and compare our results with ozonesonde data and with vertical  
170 boundary layer tracer distribution.

171

## 172 2. Observations and Methods of Analysis:

173

### 174 **2.1 *In situ* data aircraft data**

175 The *in situ* data that we use in this paper was taken from the NASA DC-8 and  
176 WB-57 by various investigators as described here. The list of chemical and  
177 physical data considered and analyzed in this paper includes ozone, carbon  
178 monoxide, methane, condensed cloud water content, organic bromine, peroxy  
179 nitric acid, calcium and methyl hydrogen peroxide. Other reactive nitrogen  
180 species are discussed more generally, but are not used for analysis because in  
181 this active convective region most reactive nitrogen species are not conserved,  
182 and these tracer relationships are chaotic.

183

184 The ozone, carbon monoxide, methane and condensed cloud water content data  
185 on the DC-8 are available at one-second-time resolution, corresponding to a  
186 horizontal resolution of about 200 m. The location of sampling for each of these  
187 constituents on the DC-8 is shown in Figure 5 of *Toon et al.* [2010]. Merged data  
188 files have been created, with all data aligned to the time stamp of water vapor  
189 data measured by the Langley DLH diode laser hygrometer, an open-path  
190 measurement without sample lag considerations. Ozone was measured using  
191 fast-response nitric oxide chemiluminescence [*Fairlie et al.* 2009, *Pearson and*  
192 *Stedman*, 1980]. Carbon monoxide and methane were measured using a  
193 tunable diode laser–based absorption technique by the Differential Absorption for  
194 CO Measurements (DACOM) instrument [*Sachse*, 1987].

195

196 Measurements of the condensed cloud water content (CWC) were made by the  
197 NCAR counterflow virtual impactor (CVI) described by *Twohy et al.* [1997].  
198 During the ER-2 and DC-8 flights that occurred on July 24, 2007, the DC-8 flew  
199 through developing convective cores with large vertical velocities and  
200 corresponding CWC. The CVI instrument, while normally accurate to within 15%  
201 (*Twohy et al.*, 1997), relies on subisokinetic enhancement of condensed water to  
202 measure low concentrations, and requires manual adjustment to measure high  
203 water contents such as are present in convective cells. Since these were not  
204 anticipated for the July 24<sup>th</sup> flight, the CVI signal was saturated twice during the  
205 flight when the DC-8 passed through convective turrets. CWC content derived  
206 from the SPEC 2DS cloud probe data [*Lawson et al.*, 2006] are also used during

207 this flight in vigorous convection, since the probe did not saturate. The 2DS  
208 integrates the cloud particle size distribution to obtain condensed water and this  
209 technique generally agreed well with the CVI measurement during the rest of the  
210 TC-4 mission.

211

212 The Meteorological Measurement System (MMS) provided accurate, high  
213 resolution pressure, temperature and wind data used in this analysis for both the  
214 DC-8 and the WB-57, using instrumentation similar to that described for the ER-2  
215 in *Scott et al.* [1990]. Ozone data from the WB-57 was measured using a dual  
216 beam ultraviolet photometer. We also compare the aircraft data with ozone data  
217 measured from sondes using electrochemical cells *Thompson et al.* and *Morris et*  
218 *al.* [2010].

219

220 We compared the vertical distribution of some other trace gases to our results  
221 from examining ozone. Methyl hydrogen peroxide (MHP) and PNA (peroxy-nitric  
222 acid) were measured using a chemical ion mass spectrometer (CIMS) technique  
223 developed at the California Institute of Technology [*Spencer et al.* 2009, *St Clair*  
224 *et al.* 2010]. Total organic bromine was calculated from individual species  
225 measured by analysis of whole air samples using gas chromatography at the  
226 University of Miami for the WB-57 and the University of California, Irvine for the  
227 DC-8. Calcium was analyzed from bulk aerosol composition measurements  
228 made from the NASA DC8 by the University of New Hampshire soluble acidic  
229 gases and aerosols (SAGA) instrument (*Dibb et al.*, 2003).

230

## 231 **2.2 Suborbital and satellite-based remotely-sensed data**

232

233 Cloud images from the Cloud Physics Lidar (CPL) on the ER-2 were used to  
234 locate aircraft measurements from the DC-8 relative to the cloud top height and  
235 cloud morphology. The CPL cloud images are a time series of 532 nm  
236 attenuated backscatter profiles, measured as described in *McGill et al.* [2002].  
237 During TC4 there were several near coincidences between overpasses by the  
238 CALIPSO satellite and the multiple-aircraft flight tracks, and we show a  
239 comparison between cloud images from the CALIOP instrument [*Winker et al.*  
240 2007], the CPL on the ER-2 and in situ CVI measurements of CWC as a movie  
241 (see section 2.3, below).

242

243 We evaluate mean tropospheric ozone volume mixing ratios calculated between  
244 the tropopause and sampling by the DC-8 that are derived using the NASA Aura  
245 Ozone Monitoring Instrument [OMI, *Levelt et al., 2006*], and the Microwave Limb  
246 Sounder (MLS). The tropospheric ozone column residual is first determined by  
247 subtracting interpolated MLS version 2.2 stratospheric column ozone [*Froidevaux*  
248 *et al., 2008*] from the OMI-TOMS [*McPeters et al., 2008*] measured column  
249 ozone for each OMI pixel. This measured column does not include ozone that is  
250 shielded from the satellite by clouds.

251

252 Ozone mean volume mixing ratio is then calculated by dividing this partial column  
253 by the difference between the tropopause pressure and the effective scene  
254 pressure ( $P_{\text{eff}}$ , in hPa) [e.g., *Ziemke et al.*, 2001, *Joiner et al.*, 2009].  $P_{\text{eff}}$  is given  
255 by:

$$256 \quad P_{\text{eff}} = (1-f)P_s + fP_c \quad (1)$$

257 In Equation 1,  $P_s$  is the surface pressure,  $P_c$  is the optical centroid cloud  
258 pressure, and  $f$  is the fraction of total radiance coming from the cloudy portion of  
259 a pixel. The optical centroid cloud pressure is derived from the OMI rotational-  
260 Raman cloud algorithm (Joiner and Vasilkov, 2006) and appropriately accounts  
261 for the shielding effect of clouds in the OMI-TOMS ultraviolet retrieval algorithm  
262 (Vasilkov et al., 2008). The initial derivation of tropospheric ozone from the OMI-  
263 MLS residual technique by Schoeberl et al. [2007] did not fully account for cloud  
264 effects. The derived column-averaged mixing ratio derived here is representative  
265 of the tropospheric column above the  $P_{\text{eff}}$ . When we extrapolate that mixing ratio  
266 to the surface, the global correlation between the OMI/MLS-derived 200 hPa to  
267 surface column ozone and that from ozonesondes improved from about 0.6 to  
268 0.8 [Joiner et al., 2009]. To our knowledge, this is the best agreement ever  
269 obtained between the ozonesonde measurements (point measurements that  
270 contain a significant amount of variability in both space and time) and satellite  
271 data that represent an average over a much larger area. This demonstrates that  
272 tropospheric ozone can be accurately derived using the residual technique in  
273 both clear and cloudy conditions.

274

### 275 **2.3 Data synthesis and analysis strategy**

276 *In situ* data from the DC-8 was merged as described above, with 1-second time  
277 resolution and a corresponding approximate horizontal resolution of 200 m. The  
278 DC-8 data set in the upper troposphere extends between 8.5 and 12.2 km, with a  
279 corresponding potential temperature range of 330-350 K. We created a DC-8  
280 data ensemble from sampling during the local “racetrack” flights with a limited  
281 geographical domain between 4-10 N latitude, and between 79 – 87 W longitude.  
282 The flights used occurred on July 17, 22, 24 and 31, and August 3, 5, and 8 of  
283 2007, and these are shown in Figure 1, with the DC-8 flight track colored by *in*  
284 *situ* ozone amount. The ER-2 flew as well on these days, with the degree of  
285 flight coordination increasing with practice as the mission progressed. Flight  
286 coordination is discussed extensively in *Toon et al.* [2010]. The WB-57 also flew  
287 a coordinated pattern during the three August flights.

288

289 Merging and interpreting the remote and *in situ* data together is challenging. We  
290 developed a special-purpose program to combine the CPL and CALIOP images  
291 and DC-8 data, as well as their geo-location and time stamp information, into  
292 geometry and scalar-data files compatible with the COTS 3-D Visualization  
293 software tool called “EnSight.” These datasets could then be co-located in space  
294 and time, with respect to a map of the Earth built from the GTOPO30 digital  
295 elevation model (DEM) and the NASA Blue Marble cloud-free image. The  
296 visualization software provided both 3-D movies and stills of the combined data  
297 set, providing a powerful and intuitive way to spatially and temporally link the

298 observations, and to build intuition for data analysis decisions. A movie showing  
299 the precise correspondence between a CALIOP cloud image from the August 5th  
300 CALIPSO overpass, the corresponding CPL cloud image from the ER-2, and in  
301 situ cloud water content from the DC-8 is shown at this link:

302 <http://tinyurl.com/tc4nasa-video01>. The vertical scale is expanded, in order to  
303 visualize detailed structures. The movie was submitted with this paper, and upon  
304 review will be archived with it.

305

### 306 3. Results and Discussion:

307

#### 308 **3.1. Overview of *in situ* observed tropospheric composition**

309 To provide an overview of the larger context of the background tropical  
310 tropospheric chemical composition of the tropical tropospheric study area, we  
311 have plotted the aggregate median vertical profile and statistical distribution of  
312 ozone and carbon monoxide, shown as Figure 2. We look at ozone and carbon  
313 monoxide because neither gas is soluble in the cloudy tropical environment, and  
314 they both have similar chemical lifetimes of about 50-60 days, much longer than  
315 the vertical mixing time of less than 1 day. The tracer data is binned at 1 km  
316 resolution, and includes all of the measurements from the DC-8 between 7S and  
317 17 N latitude, and between 70 – 90 W longitude.

318

319 The median ozone profile shows a characteristic tropical “S”-shape [Folkens,  
320 2002], with depleted ozone in the boundary layer, some ozone enhancement in

321 the middle troposphere, a minimum caused by convective outflow in the upper  
322 troposphere, between 9-10 km, and a monotonically increasing ozone gradient  
323 above the outflow maximum. In the upper troposphere, enhanced ozone of more  
324 than 65 ppbv occurs in less than 25% of the data, except above 12 km, with  
325 potential temperatures approaching or greater than 350K. Based on this, in this  
326 paper when we refer to “high” ozone, we mean specifically ozone concentrations  
327 greater than 65 ppbv. Ozone in the boundary layer is both low and strikingly  
328 uniform throughout the sample region. Correlation during boundary layer  
329 sampling with MMS wind measurements shows that ozone measured while  
330 winds have an easterly component (60 – 110 degrees) has the smallest range  
331 (19-25 ppbv), while ozone measured while winds have a southerly or westerly  
332 component has a slightly wider range (12-28 ppbv). A probability distribution of  
333 boundary layer ozone shows the median value to be about 21 ppbv, with less  
334 than 10 ppbv of variability everywhere, and no significant difference (0.5 ppbv)  
335 between the Atlantic and the Pacific marine boundary layers. This suggests that  
336 catalytic destruction of ozone by reactive hydrogen radicals (HOx) removes  
337 ozone efficiently in the lowermost atmosphere. This appears to be the case in  
338 both the marine boundary layer, and in measurements over land. Comparison  
339 with the more polluted NATIVE surface ozone data set from Las Tablas, Panama  
340 [Figure 10, *Thompson et al.*, 2010] also shows surface ozone averages near 20  
341 ppbv.

342

343 The carbon monoxide median profile is very uniform vertically, with medians  
344 between 70-90 ppbv throughout the troposphere. This contrasts with the large  
345 range of CO measured in the boundary layer, between 55-155 ppbv with the 75th  
346 percentile occurring at 90 ppbv. An examination of DACOM measurements of  
347 CO at take-off and landing at Alajuela airport shows a large amount of day-to-day  
348 variability, despite its proximity to San Jose. Comparison of the aircraft CO  
349 measurements by DACOM with surface measurements of CO from the NATIVE  
350 trailer in Panama show that the Panama site was relatively polluted, since 75% of  
351 the boundary layer aircraft measurements show CO of 90 ppbv or less, while all  
352 of the NATIVE data indicates CO of 90 ppbv or more [Thompson et. al., 2010].

353

354 Carbon monoxide is usually the product of incomplete combustion, but the  
355 convectively active TC4 region does not show much fresh pollution or biomass-  
356 burning enhancement. This is substantiated by measurements of HCN, a  
357 biomass-burning tracer that is also not enhanced above a moderate background  
358 level in the convective area. The relationship between ozone and carbon  
359 monoxide is complex, and varies by flight day. Positive correlations can indicate  
360 aged pollution or very clean air; negative correlations can indicate stratospheric  
361 influence, *in situ* ozone production from lightning NO<sub>x</sub>, biogenic influence, or  
362 fresh smoke. Because of these ambiguities, it is difficult to use the correlations  
363 to provide much useful information about air mass history. In the TC4 study  
364 region, CO is not a useful tracer for convective transport because of convective  
365 lofting of both clean and dirty lower tropospheric air. During the convective

366 “racetrack” flights, either a positive or a negative correlation between CO and O<sub>3</sub>  
367 tends to persist for all altitudes sampled, reflecting the influence of either a clean  
368 or a polluted boundary layer on an individual day. A composite CO:O<sub>3</sub>  
369 correlation plot for the mission shows no significant correlation, or any distinct  
370 plumes, indicating that a very large amount of mixing has occurred in this region.  
371 Our results suggest that care must be used in interpreting CO:O<sub>3</sub> relationships in  
372 convection over combined marine and terrestrial environments.

373

374 For context, in Figure 3 we look at the vertical ozone distribution during TC4  
375 compared with ozone measured at similar latitudes during other aircraft field  
376 missions. The comparison is facilitated because these measurements were all  
377 made using NASA Langley NO chemiluminescence detectors, with an estimated  
378 3% accuracy [Avery *et al.*, 1999, Fairlie *et al.*, 2006, Pearson and Stedman,  
379 1980]. Further, all but the ABLE-2B mission occurred during a mild ENSO cold  
380 phase. The figure shows the median ozone concentration measured in 1 km  
381 bins as a function of altitude. We show the ABLE-2A (Jul-Aug, 1985) and 2B  
382 (Apr-May, 1987) missions, with sampling over the Amazon basin and Western  
383 Atlantic, the PEM Tropics A and B (PTA Aug-Sep, 1996 and PTB Mar-Apr, 1999)  
384 missions with pan-Pacific tropical sampling, and the TRACE-P (Feb-Apr 2001)  
385 mission, which featured Asian air pollution and sampling of the Western Pacific.  
386  
387 The largest difference in tropospheric ozone appears to be seasonal, with  
388 roughly double the amount of ozone occurring in the boundary layer during July-

389 October than during February-May. This seasonal difference persists in the  
390 middle and upper troposphere, where there was about 10 ppbv more ozone  
391 measured during TC4 in July-August than there was during PTA in August-  
392 September, most likely due to the difference between sampling the remote  
393 Pacific and the TC4 study area around Central America. The TRACE-P mission  
394 was unusual in targeting Asian pollution, with a resulting high mid-tropospheric  
395 ozone median. Unfortunately, the ABLE-2A measurements do not extend higher  
396 than 5 km, but these show that ozone was a bit lower in the lower troposphere  
397 over the Amazon basin than measured during TC4. This may be because the  
398 tropical rainforest is a very efficient sink for ozone. This was discussed in detail  
399 by Gregory et. al. [1988], describing the ABLE-2A measurements. Our TC4  
400 measurements from a boundary layer leg over the Peruvian rain forest  
401 substantiate this. This boundary layer leg had the lowest average ozone  
402 concentration measured during TC4 (11 ppbv) and the highest CO (153 ppbv),  
403 produced from oxidized hydrocarbons.

404

405 Methane and ozone from TC4 are shown in Figure 4. These are mainly  
406 uncorrelated, with the exception of two plumes containing very high biogenic  
407 methane sampled in the Colombian boundary layer, once over land, and once  
408 just off the Pacific coast. The distribution looks very similar to ozone correlations  
409 with CO, and this plot is shown to illustrate the well-mixed state of the free  
410 troposphere during TC4. Methane concentrations measured at the NOAA CMDL  
411 ground stations in the Northern and Southern Hemisphere (NH and SH) closest

412 to the TC4 sample region are shown on the plot for comparison. This plot  
413 suggests that almost all of the air sampled during TC4 came from the tropical  
414 NH, with only 4% of air sampled having methane amounts less than 1750 ppbv,  
415 indicating no significant unmixed stratospheric or SH air was sampled, except  
416 during a short flight segment on August 6, the low methane “tail” in the figure.  
417 *Pfister et al.* [2010] estimate that only 10-30% of air sampled in the troposphere  
418 during TC4 comes from the NH mid-latitudes poleward of 25 N during the  
419 mission, which is consistent with this tracer data. Further, the lack of any data in  
420 the upper left quadrant of the plot with  $\text{CH}_4 < 1750$  ppbv and  $\text{O}_3 > 70$  ppbv  
421 indicates no significant stratospheric influence to the upper troposphere occurred  
422 during TC4.

423

424 Comprehensive reactive nitrogen measurements ( $\text{NO}$ ,  $\text{NO}_2$ ,  $\text{HNO}_3$ , PAN, PNA)  
425 were made from the NASA DC-8 during TC4, and we consider them here. During  
426 TC4, *Scheuer et al.* [2010] found that  $\text{HNO}_3$  was depleted on ice crystals in  
427 cirrus, and that it was enhanced in a thin layer just below cirrus by sedimenting  
428 and sublimating particles. In clouds,  $\text{HNO}_3$  is strongly anti-correlated with CWC,  
429 because it is soluble (plot not shown). In mid-latitudes near convection, *Bertram*  
430 *et al.* [2007] have reported a compelling relationship between the  $\text{NO}_x/\text{HNO}_3$  ratio  
431 in an air parcel and the time since convection lifted the air from the lower into the  
432 upper troposphere. We tried to use the reactive nitrogen data from TC4 to do a  
433 similar “convective clock” analysis. Because of the frequency of convection and  
434 the non-conservation of  $\text{HNO}_3$  in cirrus during TC4, the air parcel “age” since

435 convection cannot be determined using this method. It is likely that this method  
436 works much better in mid-latitudes than in the tropics because the frequency of  
437 convection is much less.

438

439 Further examination of the  $\text{NO}_2/\text{NO}_x$  ratio using  $\text{NO}_2$  data from OMI and lightning  
440 data by *Bucsela et al.* [2010] suggests that lightning  $\text{NO}_x$  enhancement can be  
441 between 1.5-2.5 times the  $\text{NO}_x$  background, but there is also less lightning  $\text{NO}_x$  in  
442 tropical marine convection than in midlatitude continental thunderstorms that are  
443 associated with mid-latitude fronts. The upper tropospheric relationship of  $\text{NO}_x$   
444 with  $\text{O}_3$  is uncorrelated, indicating that the production of new ozone from lightning  
445  $\text{NO}_x$  might happen downstream, but is not a dominant process within TC4  
446 maritime convection. While the ratio of total reactive nitrogen ( $\text{NO}_y$ ) to ozone has  
447 been used to indicate ozone production potential [*Ridley*, 2006], in the actively  
448 convective TC4 “racetrack” region  $\text{NO}_y$  and  $\text{O}_3$  are also uncorrelated (like  $\text{NO}_x$   
449 and  $\text{HNO}_3$ , plot not shown), and is not useful for data interpretation here. PAN  
450 observations in the TTL [*Elkins*, plot not shown] suggest that a significant amount  
451 of PAN (greater than 30 ppt) is vertically transported out of the boundary layer  
452 into the upper troposphere. PAN is not water-soluble and does not deposit on  
453 ice particles, so that reactive nitrogen can be transported vertically into the TTL  
454 and horizontally in the upper troposphere.

455

### 456 **3.2. Case studies of convective transport**

457

458 **3.2.1 July 24, 2007, the “Thor” flight**

459 On the morning of July 24, 2007, the DC-8 and the ER-2 were to sample a  
460 developing thunderstorm complex in the ITCZ system at about 5 deg N, 85 deg  
461 W. The DC-8 was to extensively sample the boundary layer in the actively  
462 developing storm, and then to ascend through the storm and to sample cirrus in  
463 the outflow region to characterize convective transport and mixing. Although the  
464 flight was a success, it was cut short by a lightning strike to the DC-8. This was  
465 the only flight during the TC4 mission that sampled the core of such an actively  
466 developing storm.

467

468 A Geostationary Operational Satellite (GOES) enhanced infrared satellite image  
469 overlain with the ER-2 and DC-8 flight tracks is shown in Figure 5a. The  
470 prevailing wind in the cirrus anvils of the convective cells is NE at 40 kt, and one  
471 can see this in the cloud pattern, as the anvils stream off to the SW. One can  
472 also see the more orderly “race track” pattern flown by the ER-2 above the cirrus,  
473 as opposed to the flight pattern taken by the DC-8 after it was hit by lightning.  
474 The cloud physics lidar (CPL), making measurements from the ER-2, provides  
475 context for the DC-8 *in situ* measurements taken inside the convective cell.  
476 Figure 5b shows a three-dimensional CPL image of the cirrus anvil, and the  
477 coincident DC-8 flight track, colored by *in situ* ozone concentration. Ozone was  
478 16 ppbv in the boundary layer (BL) beneath the storm, typical of low BL ozone  
479 measured during TC4, increasing to 30-35 ppb at 3-4 km, as expected. The CPL  
480 shows that the cirrus cloud tops extend to 14-15 km, so the DC-8 in-cloud

481 sampling occurred at about 3-4 km below the tropopause. One can see that the  
482 cirrus are ragged and uneven, and that the ozone inside them is highly variable,  
483 between 30 and 75 ppbv.

484

485 The DC-8 sampled inside the developing cloud anvils at 11 km, 225 hPa, and  
486 penetrated the core of the storm where the ambient temperature was -47  
487 degrees C, so the cloud particle phase was ice. The 2DS cloud probe measured  
488 very large spikes in the condensed water content during this segment of the  
489 flight, when the DC-8 passed through strong convective turrets, shown in Figure  
490 6. This figure also shows the large vertical velocity of 20 m/s that was measured  
491 by MMS.

492

493 A simple calculation of ozone production is possible in this very fresh convection.  
494 Using TC<sup>4</sup> measured ozone production rates of 1.1-3.2 ppbv/hour (*Morris et al.*  
495 [2010]), with 2 m/s as a typical mean vertical velocity occurring over a vertical  
496 transport distance of 10 km, only 0.75-4.4 ppbv of ozone can be made during  
497 vertical transport. This is much smaller than the 14-19 ppbv difference between  
498 the low O<sub>3</sub> mixing ratios of 30-35 ppbv measured in the convective cloud and BL  
499 O<sub>3</sub> of 16 ppbv. The higher O<sub>3</sub> mixing ratios measured in the turrets also indicate  
500 that this air was not transported from the boundary layer without significant  
501 mixing to 10-11 km (225 hPa), where our sampling occurred. O<sub>3</sub> generation by  
502 electrical corona discharge may be possible [Minschwaner, 2008]. This process  
503 is still somewhat speculative, and Minschwaner et. al. estimate a total generation

504 of  $2 \times 10^{28}$  molecules of O<sub>3</sub> in the highly electrified storm they studied, which is  
505 not enough to account for the O<sub>3</sub> difference between TC<sup>4</sup> BL and convective  
506 cores.

507

508 Figure 7 shows a time series of tracers measured while the DC-8 sampled the  
509 convection at 10-11km. This corresponds to the upper two “loops” shown in  
510 Figure 5b, which also shows the large inhomogeneity of the convective cloud.  
511 There is a striking anti-correlation between CWC and ozone, with high ozone  
512 values (65-70 ppb) measured where CWC is low (“no cloud”), and lower ozone  
513 values (30-35 ppbv) measured inside the clouds. Positive vertical winds (Figure  
514 are also anti-correlated with ozone. This strong anti-correlation between ozone  
515 and clouds persists throughout the TC4 data set.

516

517 There is a positive correlation during this flight between carbon monoxide and  
518 ozone, indicating some aged pollution in the upper tropospheric background air,  
519 and vertical advection of relatively clean lower tropospheric air. However, this  
520 result is not consistent during upper tropospheric sampling on other flights.

521 Correlations between ozone and horizontal wind direction, and between ozone  
522 and oxides of nitrogen are not significant during this flight (not shown), nor are  
523 they significant during the “racetrack” sampling in the upper troposphere for the  
524 mission as a whole. This indicates that convection dominates in redistributing  
525 ozone, and in this region it is more significant as a process for creating ozone  
526 variability than horizontal advection and *in situ* photochemistry.

527

528 While relatively low ozone concentrations in the upper troposphere can be an  
529 effective indication of convective influence, this argument needs to be  
530 complemented by examining concentrations of a “positive” tracer for convection.  
531 Methyl hydrogen peroxide ( $\text{CH}_3\text{OOH}$ , MHP) is a convenient convective tracer to  
532 use in this case, because it is enhanced in the lowermost atmosphere but it is not  
533 significantly soluble. *Cohan et al.* [1999] have shown that MHP in very fresh  
534 convection can be elevated up to 6 times over the upper tropospheric  
535 background, but decays in the upper troposphere with a chemical lifetime of 1-2  
536 days.

537

538 Figure 7 shows  $\text{CO}$ ,  $\text{O}_3$ , MHP and pernitric acid, ( $\text{NO}_2\text{HO}_2$ , PNA) measured  
539 during two of the 11 km (225 hPa) sampling loops, along with averages obtained  
540 just prior to the ascent during the boundary layer run. The addition of the tracers  
541 shows that three distinct air types were sampled. Air that has recently been  
542 transported into the upper troposphere with low  $\text{O}_3$  has high MHP and low PNA.  
543 This freshly convected air can be seen at 14:05 and 15:10 GMT, corresponding  
544 to the DC-8 passage through convective turrets shown in Figure 6. The second  
545 air type, background tropospheric air with high  $\text{O}_3$  mixing ratios ( $> 60$  ppb) has  
546 relatively high PNA and low MHP, with examples centered near 14:59 and 15:07  
547 GMT on the plot. There are also slightly higher values of  $\text{CO}$  and  $\text{CH}_4$  (not  
548 shown) that are anti-correlated with  $\text{O}_3$ , with examples at around 15:17 and 15:38  
549 GMT on the plot.

550

551 Figure 8 shows the flight track from above, indicating the location of these  
552 different air types, which stay coherent between flight loops. The ozone color  
553 scale in this plot is the same as shown in the 3-D image in Figure 5B. The  
554 variability has spatial scales of the order of 10-50 km. Figure 8 also shows  
555 approximate footprint sizes of various ultraviolet and visible satellite backscatter  
556 instruments. The smallest is that of OMI, with a nadir pixel of approximately 12  
557 km x 24 km. The spatial scales of the different observed air types are similar to  
558 the OMI nadir footprint, so it is feasible that OMI data can resolve ozone  
559 variability that is caused by convective processes, and the data has been used  
560 previously to retrieve ozone mixing ratios inside deep convective clouds [*Ziemke*  
561 *et al.*, 2009].

562

563 The mean tropospheric ozone volume mixing ratios (ppbv) calculated between  
564 the tropopause and 300-450 hPa derived using OMI and Microwave Limb  
565 Sounder (MLS) data are shown in Figure 9a for the AURA overpass occurring  
566 closest to this flight (18:30 Z on July 24, 2007). This overpass occurred about 4  
567 hours after the DC-8 sampled inside the developing convection as described  
568 above. Examination of GOES images using loops provided by the Langley TC4  
569 satellite group [*Minnis*, 2010] shows that during this time the convective system  
570 continued to grow, with outflow streaming off to the southwest. Figure 9b shows  
571 the reflectivity measured by OMI during the AURA overpass, and shows the  
572 location of the cloud anvil. The DC8 flight path while the plane was circling near

573 the tops of the convective clouds is shown on both plots. In this area there is a  
574 large contrast in mean ozone mixing ratios from < 40 ppbv (blues) to >65 ppbv  
575 (reds).

576

577 These derived OMI column-mean mixing ratios appear to be consistent with the  
578 in situ measurements taken several hours earlier in the developing storm,  
579 showing variability due to the contrast between ozone mixing ratios in freshly  
580 lofted and background upper tropospheric air. The OMI data suggests a region of  
581 relatively polluted air adjacent to the cloud, with ozone mixing ratios similar to  
582 measurements with elevated CO from the DC-8 (Figure 7). Lower ozone seen  
583 by OMI in the SW corner of the scene corresponds to the convective outflow  
584 region of the cloud, as verified by GOES image loops and the prevailing NE wind.  
585 As expected, OMI/MLS data does not capture the finer-scale ozone variability  
586 shown in the *in situ* measurements. However, the larger perspective that OMI  
587 offers shows the extent of lowered ozone in the convective outflow to the  
588 southwest of the system. A histogram of the OMI mean tropospheric ozone  
589 measurements for the entire region peaks at 49 ppbv (+/- 10 ppbv), which is  
590 consistent with the *in situ* ozone distribution shown in Figure 2a, and is indicated  
591 in the clear regions of Figure 9a. Further, in the “racetrack” region the maximum  
592 and minimum ozone mixing ratios of ~70 ppbv and ~35 ppbv retrieved using the  
593 OMI data are similar to those measured *in situ* from the DC-8 (Figure 7). Since  
594 sonde and lidar ozone data is not available in deep convective clouds, this

595 comparison of *in situ* and OMI ozone measurements provides a unique validation  
596 of the OMI/MLS mixing ratios derived inside convection.

597

### 598 **3.2.2 August 5, 2007, Convective Outflow**

599 On this day DC-8, ER-2 and WB-57 flew a well-coordinated pattern in convective  
600 outflow, first identified in satellite images. In section 2 we presented a movie  
601 showing the relationship between the DC-8 flight track and the cirrus outflow from  
602 the convection sampled, including images of the cirrus from both the CALIOP  
603 instrument on CALIPSO and the CPL. Figure 10 focuses on measurements from  
604 the DC-8. Panel a shows a 3-dimensional picture of the CPL cirrus image and  
605 in-situ ozone data (bottom) and the *in situ* carbon monoxide data (top). During  
606 this flight the boundary layer and lower troposphere are quite polluted compared  
607 with the July 24<sup>th</sup> flight shown above, and on this day, O<sub>3</sub> and CO are almost  
608 always anti-correlated, as opposed to their positive correlation on July 24.

609

610 The 3-dimensional picture shows that the highest DC-8 racetrack pattern was  
611 flown inside the cirrus, 3-4 km below the anvil tops at 14-15 km. Panel b shows  
612 the O<sub>3</sub>, CO and CWC traces from the racetrack sampling. The spikes of higher  
613 ozone (60 ppbv) coincide with lower CO (90 ppbv) on the side of the racetrack  
614 where the DC-8 turns around outside of the cloud, as indicated by the absence of  
615 CWC. This trace is shown because it is a good example of vertical advection of  
616 polluted air out of the boundary layer, and of the in cloud/out of cloud difference  
617 in air composition. Panel c is a plot of O<sub>3</sub> (y-axis) vs. CWC (x-axis) from the

618 whole flight, colored by altitude. It is interesting to note the predominance of O<sub>3</sub>  
619 concentrations of ~ 25 ppbv in the lower clouds, and O<sub>3</sub> ~ 35-40 ppbv in the anvil  
620 clouds. This again suggests that convection does not transport undiluted air  
621 directly into the upper troposphere.

622

### 623 **3.3 Regional statistics**

624 In this section we look at the combined data set from all of the local upper  
625 troposphere (8-12 km) sampled during TC4. Figure 11 shows the O<sub>3</sub>:CWC  
626 relationship in all the data colored by altitude, similar to Figure 10c. The cloudy  
627 areas clearly have less ozone than the clear ones, with all of the high ozone  
628 occurring where CWC approaches zero. A somewhat arbitrary value of 0.01  
629 g/m<sup>3</sup> was chosen to divide the data set into “cloudy” and “not cloudy” bins for  
630 looking at ozone probability distributions. The CVI out-of-cloud baseline is lower  
631 than this (~0.002 g/m<sup>3</sup>), but a higher value is chosen to avoid including a CVI  
632 cloud exit hysteresis signal as a cloud. The ozone distribution is not very  
633 sensitive to this choice, tested between 0.002 – 0.02 g/m<sup>3</sup>.

634

635 Figure 12 a and b show “in cloud” and “out of cloud” probability histograms of  
636 ozone and carbon monoxide. The peak of the in-cloud probability distribution  
637 occurs at 37 ppbv, which is representative of in-cloud O<sub>3</sub> mixing ratios measured  
638 in both active convection and convective outflow as shown above. There are  
639 relatively few measurements of O<sub>3</sub> between 50-75 ppbv in the cloudy data. The  
640 small peak in O<sub>3</sub> at 80 ppbv in cloud did not reach the upper troposphere by

641 vertical transport directly from the lower troposphere, because there were no  
642 measurements of ozone greater than 75 ppbv below 10 km. The DC-8 must  
643 have flown through a small, cloudy pollution plume, but there are so few data  
644 points that this small plume does not affect our conclusions significantly.

645

646 In contrast, the “out of cloud” ozone measurements in the upper troposphere  
647 show ozone concentrations between 50-75 ppbv in about 50% of the air  
648 sampled. The CO histograms show a peak in “clean” air with CO of 75 ppbv  
649 outside of the clouds, perhaps representing a tropical upper tropospheric  
650 background. There is a somewhat more even distribution of CO occurring in  
651 clouds, reflecting the large amount of variability in CO in the lower troposphere.  
652 The cloudy air contains more CO than the clear air, indicating that vertical  
653 convective transport is a net source of “dirty” air to the upper troposphere.

654

### 655 **3.4 Comparison with sondes and tracer profiles**

656 An analysis of vigorous tropical convection in the Western Pacific by *Solomon et*  
657 *al.* [2005] documents the transport of air containing very low ozone to the tropical  
658 TTL region, and also shows the usefulness of examining a profile of low ozone  
659 measurements for establishing the altitude of maximum convective outflow.

660 From our analysis of in cloud and out of cloud probability distributions of ozone  
661 measured in the upper troposphere, we find a minimum in the histogram  
662 occurring at 44 ppbv, with a sharp peak in the cloudy mixing ratios below this  
663 value (Figure 12a). Using this number as a threshold for “low ozone”, we

664 calculate the fraction of measurements of low ozone in 500 m bins throughout  
665 the troposphere for the Panama and Alajuela sondes, as well as for the WB-57  
666 and DC-8 local ozone profiles. This distribution is shown in Figure 13a. For  
667 comparison, Figure 13b shows this distribution with a threshold of 28 ppbv, the  
668 largest ozone mixing ratio measured during DC-8 boundary layer runs.

669 There is a large difference between the sonde and the aircraft low ozone  
670 measurement distributions, which we attribute to a sampling difference. The  
671 sondes were mainly launched in background air, and the planes targeted  
672 convection, so the difference is between clear and cloudy air. The DC-8  
673 distribution peaks just below 10 km, while the WB-57 peaks just above, and this  
674 is most likely because of the extensive DC-8 in cloud sampling. Evident from  
675 both figures is that convective outflow peaks at 10-11 km, a lower altitude in this  
676 region than in the Western Pacific. This is consistent with an average cloud top  
677 height of 14.2 km derived from the CPL data [*Chang et al., this issue*], also lower  
678 than the Western Pacific. Figure 13b also indicates that only 5-10% of air  
679 sampled in the maximum outflow region comes directly from the boundary layer  
680 without mixing.

681  
682 Given the difference between sonde and aircraft measurements of maximum  
683 convective outflow, we looked more carefully at the distribution of MHP. The  
684 altitude profile of MHP for all TC4 local flights is shown in Figure 14, with the  
685 upper tropospheric maximum occurring at 10-11 km, substantiating the aircraft  
686 measurements of low ozone. For comparison to fresh convective

687 measurements, the inset (Figure 14b) is a correlation plot of O<sub>3</sub> and MHP  
688 measured during the July 24 case study. With the exception of 4-5 data points,  
689 all of the elevated MHP (> 300 pptv) occurs at ozone mixing ratios of less than 40  
690 ppbv. During this flight the distributions of MHP in the boundary layer (O<sub>3</sub> ≤ 20  
691 ppbv), above the boundary layer in the lower troposphere (2-3 km, O<sub>3</sub> ~ 30  
692 ppbv), and in the upper tropospheric cloudy measurements are similar. The  
693 highest uncertainty of the MHP measurements occurs in humid air, i.e., the  
694 marine boundary layer.

695

696 We also tested the profile of another low altitude tracer measured from the DC-8  
697 and WB-57, in this case the total of measurements of organic bromine species  
698 that are produced by marine life in the ocean surface waters. Figure 15a shows  
699 a composite of total organic bromine measurements. It is evident from the  
700 organic bromine enhancement in the upper troposphere that the altitude of  
701 maximum convective outflow occurs at 10-11 km. For comparison, Figure 15b  
702 shows the profile of calcium ions measured in bulk aerosol samples as a proxy  
703 for dust. In regions impacted by Saharan dust, dust is enhanced in nearby cirrus  
704 (Karl Froyd, personal communication). Since the Saharan dust layer is typically  
705 found at 2-3 km, this would suggest a significant contribution to convective  
706 outflow from this altitude, consistent with what we find most likely using ozone.  
707 Very simple mass-balance calculations using ozone, bromine and calcium  
708 measurements at 10-11 km suggest that about 50% of the mass in this region of

709 the upper troposphere has been transported upwards from the lower  
710 troposphere.  
711  
712 All ozone measured in the upper troposphere above 6 km is > 30 ppbv, with  
713 medians > 40 ppbv, and all boundary layer ozone measurements during TC<sup>4</sup> are  
714 < 27 ppbv with a 20 ppbv median. Either boundary layer air is mixing perfectly  
715 with mid-tropospheric air (O<sub>3</sub> ~ 45 ppbv) during the rapid ascent to 10 -11 km, or  
716 more likely the convection is lofting a significant amount of air from above the BL,  
717 which has also been observed to happen in continental thunderstorms [Pickering,  
718 1988]. This is supported by the temperature and dewpoint soundings from  
719 sondes launched from the DC-8 into the convective clouds during racetrack  
720 flights. Skew-T plots from these soundings show that while there is always a  
721 wind shear defining the top of the boundary layer, often the temperature  
722 inversion is negligible and air is at or very near saturation up to 500-600 hPa (3-  
723 5.5 km), where there is frequently another small temperature inversion. Further  
724 examination of MMS vertical velocities in convection show well-defined peaks in  
725 positive vertical velocities (>2 m/s) occurring at pressures of 820, 680, 460 and  
726 225 hPa in the developing 07/24 convection, and at 800 and 600 hPa in the more  
727 mature convective cell sampled on 08/05. Mass conservation implies that  
728 compensating convergence or entrainment is also occurring at these altitudes.

729

730 Summary:

731 The ITCZ is a region of complex diabatic processes and small-scale mixing, and  
732 typically general circulation models do not perform well in this environment.  
733 Extensive sampling of the convectively active upper tropospheric ITCZ during  
734 TC<sup>4</sup> by multiple aircraft provides a unique opportunity to use observations to  
735 understand convective transport processes. We found the troposphere to be  
736 well-mixed tropical background air with well-aged pollution, no distinct plumes of  
737 stratospheric air and very few plumes of freshly polluted air. Due to the  
738 frequency of convection and cloud processing of air, reactive nitrogen ratios are  
739 not effective in this region for studying convective processes. Further, since both  
740 clean and dirty BL air is lofted in this region, use of CO as a convective tracer is  
741 problematic. By examining aircraft data from two flight days during which the  
742 ER-2 and the DC-8 sampled an actively developing convective system, and a  
743 more mature system generating convective outflow, we find that the most robust  
744 relationship is an anti-correlation between ozone and the amount of condensed  
745 water in a convective cloud.

746

747 When we extend this analysis to a combined data set from DC-8 sampling of the  
748 upper troposphere in the “racetracks” pattern, we find that the peak of the ozone  
749 measurement distribution in cloud is 37 ppbv. Carbon monoxide measurements  
750 imply that there is a net transfer of polluted air from the lower to the upper  
751 troposphere. Boundary layer ozone measurements are tightly distributed around  
752 20 – 22 ppbv, lower than the value found in convective clouds by roughly 15  
753 ppbv. Measurements of vertical velocity in active convection and Lagrangian

754 measurements of the ozone production rate from a sonde in convection imply  
755 that although the ozone production rate can be large, it is probably not capable of  
756 adding the missing 15 ppbv of ozone during transport. Measurements of methyl  
757 hydrogen peroxide do not help to discriminate between transport of air from  
758 above the boundary layer into the upper troposphere, and boundary layer air that  
759 has mixed significantly (50%) during the rapid (~15-20 minutes) vertical transport  
760 to 10-11 km. We note that the sensitivity of MHP measurements in humid air,  
761 and therefore the lower troposphere, is relatively poor. However, vertical velocity  
762 profiles, temperature and dewpoint soundings, and the lack of ozone < 28 ppbv  
763 in convective outflow suggest that entrainment of air and rapid vertical transport  
764 from above the boundary layer is more likely.

765

766 The altitude of maximum convective outflow measured during TC4 is found to be  
767 between 10-11 km, characterized by the maximum probability of measuring low  
768 ozone, and maximums in the vertical distributions of MHP and total organic  
769 bromine. This is significantly lower than predicted by the theoretical model of  
770 *Folkins et al.* [2006], which calculates the maximum amount of flux divergence to  
771 occur at 12 km, but is consistent with cloud top heights that are also lower (14.2  
772 km, *Chang, this issue*), so that in both cases the altitude of maximum convective  
773 outflow occurs about 4 km below the cloud tops. Similarly, it is also lower than  
774 indicated by measurements from sondes in the Western Pacific [*Solomon et al.*,  
775 2005]. A rough mass balance calculation of the amount of convective transport  
776 using mean ozone, bromine and calcium ions (“dust”) suggests that 50% of the

777 air in the upper troposphere below the TTL in this region has been vertically  
778 transported there by convection. There does not appear to be a significant  
779 amount of undiluted boundary layer air being vertically transported to the upper  
780 troposphere, even in very active convection

781

782 Acknowledgements:

783 The authors thank the NASA Middle Atmosphere and Tropospheric Chemistry  
784 Programs for funding, and Program Managers Michael Kurylo and Hal Maring for  
785 launching sondes from the DC-8. We thank Lenny Pfister for all sorts of  
786 meteorological information and consultation. We thank Gary Morris for providing  
787 the Las Tablas sonde data, and we thank Alex Bryan and David Lutz for  
788 launching all of these Panama sondes. Holger Voemel provided the Alajuela  
789 ozonesonde data, and Ru-shan Gao provided ozone measurements from the  
790 WB-57. Ross Salawitch and Tim Canty provided the plot of total organic  
791 bromine, and we are grateful for many helpful discussions. We also thank Mario  
792 Rana for DC-8 fast-response tracer lag correlations and Ali Aknan for “Chemical  
793 Digital Atlas” plots and calculations of statistical vertical tracer distributions during  
794 various tropospheric aircraft field missions ([http://www-air.larc.nasa.gov/cgi-](http://www-air.larc.nasa.gov/cgi-bin/datlas)  
795 [bin/datlas](http://www-air.larc.nasa.gov/cgi-bin/datlas)). We are grateful to K.A. Masserie and E. Dlugokencky at NOAA  
796 CMDL for the Barbados and Bahia methane measurements, and to Pat Minnis  
797 and his group for the GOES satellite images and loops.

798 Keywords:

799 Convection, tropics, ITCZ, vertical transport, chemical tracers, ozone, condensed  
800 cloud water content  
801

802 Figure Captions:

803

804 **Figure 1:** TC4 local “racetrack” flights: Flight tracks of the NASA DC-8 are  
805 shown from above, colored by the amount of *in situ* ozone measured along the  
806 way. The flight tracks shown here represent the location of data collected and  
807 used in this paper for analysis of the convective outflow region in the upper  
808 troposphere. During these flights the DC-8 flight planning featured extensive  
809 sampling of active convection or convective outflow in close proximity to the  
810 aircraft home base in Alajuela, Costa Rica. Many of the flights show a  
811 characteristic “racetrack” pattern, maintained while 2 or 3 planes were stacked  
812 vertically.

813

814 **Movie:** The movie, “Integrated Cloud Observations on August 5, 2007”, shows  
815 the 3-dimensional spatial and temporal relationships between *in situ* DC-8,  
816 remote ER-2 and A-Train satellite sampling of a convective cloud on August 5,  
817 2007 during the NASA Tropical Clouds, Composition and Climate Coupling (TC4)  
818 experiment. At the beginning of the movie, the DC-8 takes off from Alajuela,  
819 Costa Rica. The DC-8 flight track in this movie is colored by condensed cloud  
820 water content (CWC), measured by the counterflow virtual impactor. The scale  
821 for CWC is shown on the right hand side of the movie screen, and is blue in clear  
822 air. The DC-8 samples the boundary layer and the lower tropospheric inflow  
823 region near a large convective cloud when it is joined by the ER-2, flying  
824 overhead. The ER-2 carries the cloud physics lidar (CPL), which provides an

825 image of backscattered light from cloud particles as a moving curtain with the  
826 DC-8 flying up through it. Coloration of the DC-8 track shows where it is sampling  
827 in the cloud. Finally, a CALIPSO satellite overpass occurs at the end of the  
828 aircraft sampling, providing a CALIOP lidar backscatter image of the cloud from  
829 space. Rotation of the scene at the end of the movie shows the cloud structure  
830 in 3 dimensions, and the striking coincidence between the two lidar backscatter  
831 images of the cloud.

832

833 **Figure 2:** TC4 Ozone and Carbon Monoxide Median Profiles: This figure shows  
834 profiles of the median, the first and third quartile (green boxes), and the 5%-95%  
835 distribution (whiskers) of the *in situ* ozone and carbon monoxide measured from  
836 the NASA DC-8 by FASTOZ and DACOM during TC4. Data taken between 7S  
837 and 17N latitude, and between 70-90W longitudes, is averaged to 30 seconds  
838 and binned in 1 km intervals for all the TC4 flights.

839

840 **Figure 3:** Profiles of the median ozone concentration calculated using 30 second  
841 averaged data sampled between 7S and 17 N latitude during various aircraft field  
842 missions over the tropical Pacific and Western Atlantic oceans. The data is  
843 binned at 1 km vertical resolution, and extends over the same latitudinal range of  
844 the tropics as does the TC4 mission. The historical data is shown as context for  
845 comparison with the TC4 data, which is shown in green. Data from each mission  
846 is annotated with a color-coded label listing the mission timeframe.

847

848 **Figure 4:** A plot of ozone concentrations are shown versus methane measured  
849 using the DACOM instrument. They are uncorrelated, and this reflects how well  
850 mixed the air is in the TC4 study area of active tropical convection. NOAA CMDL  
851 measurements of methane from the closest Southern and Northern Hemispheric  
852 surface sampling stations are shown for comparison with the aircraft  
853 measurements. There is no stratospheric air, which would appear in the upper  
854 left corner of this plot.

855

856 **Figure 5:** This figure is a composite of images from July 24, 2007, when the DC-  
857 8 flew underneath the ER-2 through a developing convective system and was hit  
858 by lightning. Panel a is a GOES visible image showing clouds during the high-  
859 altitude portion of the DC-8 flight through active convection. The DC-8 (blue) and  
860 ER-2 (red) flight tracks are superimposed on this image, which was provided by  
861 Patrick Minnis, NASA Langley. Panel b is a 3-dimensional view of the CPL lidar  
862 image of cloud tops and the DC-8 track (colored by ozone) through the storm.  
863 The image shows low ozone in the boundary layer (16 ppbv), moderate ozone in  
864 the lower troposphere, and large variability in ozone sampled in the racetrack  
865 loops 3-4 km below the cloud tops.

866

867 **Figure 6:** Panel a of his figure shows a photograph from the DC-8 forward-  
868 looking video that shows convective turrets in the vigorous convection sampled  
869 on July 24, 2007. The second panel shows data from 11 km in the location of the  
870 green arrow in the video still. The vertical velocity was measured *in situ* by the

871 MMS on the DC-8, in red, and ice water content (black) and particle density  
872 (blue) were measured by the 2D-S cloud probe. The peak vertical velocity of 20  
873 m/s occurs with the large ice water concentration of 2.4 g/m<sup>3</sup>, indicated on the  
874 plot.

875

876 **Figure 7:** Time series of condensed cloud water content (blue), ozone (black),  
877 carbon monoxide (red), methyl-hydrogen peroxide, CH<sub>3</sub>OOH (orange) and  
878 peroxy-nitric acid, HO<sub>2</sub>NO<sub>2</sub> (purple) during racetrack portion of the 24 July flight  
879 in actively developing convection. The scale for the condensed cloud water  
880 content measured by the CVI and 2DS instruments is on the right-hand side, in  
881 g/m<sup>3</sup>. Ozone, CWC and CH<sub>3</sub>OOH are anti-correlated, while CO and HO<sub>2</sub>NO<sub>2</sub> are  
882 positively correlated with O<sub>3</sub>.

883

884 **Figure 8:** Map (degrees latitude and longitude) of the racetrack portion of the  
885 flight, colored by ozone using the same scale as shown in the 3-D image in  
886 Figure 5b. The black boxes show approximate nadir footprints of OMI (smallest),  
887 SCIAMACHY (medium), and GOME2 (largest).

888

889 **Figure 9:** Panel a shows OMI/MLS tropospheric ozone mean volume mixing ratio  
890 (units ppbv) measured during the 18:30 Z overpass of the AURA satellite on July  
891 24, 2007. The OMI swath is 2600 km wide. Panel b shows the corresponding  
892 OMI reflectivity measurements, and the DC-8 flight path for this day is shown on  
893 both panels. These OMI measurements correspond to the detailed aircraft tracer

894 measurements taken from the DC-8 was circling near 225 hPa inside the active  
895 convective system that are shown in Figures 7 and 8. A loop of GOES satellite  
896 images (not shown) clearly shows the convective outflow streaming off to the  
897 SW, coincident with the lower O<sub>3</sub> values measured by OMI.

898

899 **Figure 10:** Several plots of ozone, CO, condensed cloud water and cloud images  
900 are shown here from the August 5<sup>th</sup> flights of the DC-8 and ER-2. These images  
901 correspond to the movie showing the 3-dimensional CALIOP, CPL and DC-8  
902 cloud data all together. Figure 10a is a 3-dimensional still image of the entire  
903 DC-8 and ER-2 flights. The CPL shows the location of the cirrus anvils sampled,  
904 with cloud tops at 14 km, 3-5 km above the DC-8. The DC-8 flight track is  
905 colored by *in situ* ozone. Overlain above this image is a repeated DC-8 flight  
906 track, colored by carbon monoxide. Figure 10b shows the time series of CO  
907 (red) ozone (black) and CWC (blue) from the DC-8 during the racetracks. The  
908 trace shows spikes of high ozone and lower CO on the dry side of the racetrack,  
909 outside of the cirrus anvil. Figure 10c is a correlation plot of ozone and  
910 condensed cloud water, colored by altitude.

911

912 **Figure 11:** A composite correlation plot of ozone and condensed cloud water  
913 content measured by the CVI instrument in the upper troposphere during all of  
914 the “racetrack” flights is shown here. The data points are colored by altitude.

915

916 **Figure 12:** Shown in Figure 12a are normalized probability distribution  
917 histograms for ozone data measured during upper tropospheric “racetracks”  
918 when the DC-8 was in a cloud (blue) and not in a cloud (red). A threshold of 0.01  
919 g/m<sup>3</sup> of equivalent liquid condensed cloud water was chosen to divide the data  
920 set. The choice of this threshold is described in the text. Normalized probability  
921 distributions for carbon monoxide inside (blue) and outside (red) of clouds are  
922 shown in Figure 12b, similar to Figure 12a for ozone.

923

924 **Figure 13:** This figure shows a profile of the probability of occurrence of low  
925 ozone in 500 meter vertical bins for the WB-57 and the DC-8 TC4 ozone data  
926 from local flights, and for the Alajuela and Panama sonde measurements. Panel  
927 “a” shows the probability of measuring  $O_3 < 44$  ppbv, a threshold derived from the  
928 probability distribution shown in Figure 12 to include the “in cloud” low ozone  
929 peak. For comparison, panel “b” shows  $P(O_3 < 28$  ppbv), which includes all  
930 measured boundary layer values, but less than 25% of ozone measured at 2 km  
931 and above.

932

933 **Figure 14:** Altitude profile of MHP mixing ratio as measured from DC8 in all local  
934 flights during TC4. Gray crosses are individual (1 s) points. Red trace is the  
935 median of 1-km altitude bins; whiskers show the first and third quartiles for these  
936 bins. For comparison, the inset is a correlation plot of  $O_3$  and MHP from the July  
937 24 flight in very fresh, developing convection.

938

939 **Figure 15:** Panel “a” of this figure is the profile of total organic bromine measured  
940 by gas chromatography performed on whole air samples taken from the NASA  
941 ER-2 and the DC-8 during the TC4 field campaign. Total organic bromine is  
942 shown here as a tracer for boundary layer air. Panel “b” shows an aggregate  
943 profile of calcium ion concentrations taken from all available bulk air samples  
944 taken during the TC4 local flights. Calcium is used as a proxy for Saharan dust.  
945  
946

947 References:

948

949 Bertram, T., et. al., Direct measurements of the convective recycling of the upper troposphere,  
950 *Science*, 315, 816-820, doi:10.1126/science.1134548, 2007.

951

952 Bucsela, E., et. al. (2010), Lightning-generated NO<sub>x</sub> seen by OMI during NASA's TC4  
953 experiment, *J. Geophys. Res.*, this issue.

954

955 Burrows, J.P., E. Hölzle, A.P.H. Goede, H. Visser, W. Fricke, SCIAMACHY- Scanning Imaging  
956 Absorption Spectrometer for Atmospheric Chartography, *Acta Astronautica*, 35, 445, 1995.

957

958 Callies, J., E. Corpaccioli, M. Eisinger, A. Hahne and A. Lefebvre, GOME-2 - MetOp's Second  
959 Generation Sensor for Operational Ozone Monitoring, *European Space Agency Bull.*, 102,  
960 2000.

961

962 Dibb, J., et al., 2003. Aerosol chemical composition in Asian continental outflow during TRACE-P:  
963 comparison to PEMWest B. *J. Geophys. Res.* 108 (D21), 8815.

964

965 Fairlie T. D., M. A. Avery, R. B. Pierce, J. Al-Saadi, J. Dibb, G. Sachse (2007), Impact of  
966 multiscale dynamical processes and mixing on the chemical composition of the upper  
967 troposphere and lower stratosphere during the Intercontinental Chemical Transport  
968 Experiment–North America, *J. Geophys. Res.*, 112, D16S90,  
969 doi:10.1029/2006JD007923.

970

971 Folkins, I., P. Bernath, C. Boone, L.J. Donner, A. Eldering, G. Lesins, R.V. Martin, B.-M.  
972 Sinnhuber, and K. Walker (2006), Testing convective parameterizations with tropical  
973 measurements of HNO<sub>3</sub>, CO, H<sub>2</sub>O, and O<sub>3</sub>: Implications for the water vapor budget, *J.*  
974 *Geophys. Res.*, Vol. 111, D23304, doi:10.1029/2006JD007325.

975

976 Folkins, I., P. Bernath, C. Boone, K. Walker, A.M. Thompson, and J.C. Witte, The seasonal  
977 cycles of O<sub>3</sub>, CO and convective outflow at the tropical tropopause, *Geophys. Res. Let.*, 33,  
978 L16802, doi:10.1029/2006GL026602.

979

980 Folkins, I., C. Braun, A.M. Thompson, J.C. Witte (2002), Tropical ozone as an indicator of deep  
981 convective outflow, *J. Geophys. Res.*, 107, D13, doi: 10.1029/2001JD001178.

982

983 Folkins, I., M. Lowenstein, J. Podolske, S.J. Oltmans, and M. Profitt (1999), A barrier to vertical  
984 mixing at 14 km in the tropics: Evidence from ozonesondes and aircraft measurements, *J.*  
985 *Geophys. Res.*, Vol. 104(D18), 22095-22102.

986

987 Froidevaux L, Y. B. Jiang, A. Lambert, et al. (2008), Validation of Aura Microwave Limb Sounder  
988 stratospheric ozone measurements, *J. Geophys. Res.*, 113, D16, D16S41,  
989 doi:10.1029/2007JD008771.

990

991 Gregory, G.L., C.H. Hudgins, J. Ritter and M. Lawrence (1987), In situ ozone instrumentation for  
992 10-Hz measurements: Development and evaluation, Proceedings of sixth symposium on  
993 Meteorological Observations and Instrumentation, New Orleans, LA, Jan 12-16, 136-139.

994

995 Gregory, G., et. al. (1988), Boundary layer ozone: An Airborne Survey Above the Amazon Basin,  
996 *J. Geophys. Res.*, Vol 93(D2), 1452-1468.

997

998 Heymsfield, G.M., L. Tian, A.J. Heymsfield, L. Li, and S. Guimond (2009), Characteristics of deep  
999 tropical and subtropical convection from nadir-viewing high-altitude airborne Doppler radar, *J.*  
1000 *Atmos. Sci.*, in press.

1001

1002 Hlavka, D., L. Tian, W. Hart, L. Li, M. McGill, and G. Heymsfield (2010), Vertical cloud climatology  
1003 during TC4 derived from high-altitude aircraft merged lidar and radar, *J. Geophys. Res.*, this  
1004 issue.

1005

1006 Joiner J., and A. P. Vasilkov (2006), First results from the OMI rotational Raman scattering cloud  
1007 pressure algorithm, 44, 5, 1272-1282.

1008

1009 Joiner, J., M. R. Schoeberl, A. P. Vasilkov, et al. (2009), Accurate satellite-derived estimates of  
1010 the tropospheric ozone impact on the global radiation budget, *Atmos. Chem. Phys.*, 9, 13,  
1011 4447-4465.

1012

1013 Kley, D., P.J. Crutzen, H.G.J. Smit, H. Vomel, S.J. Oltmans, H.R. Grassi, and V. Ramanathan  
1014 (1996), Observations of near-zero ozone concentrations over the convective Pacific – effects  
1015 on air chemistry, *Science*, 274, 230-233.

1016

1017 Lawson, R.P., E.J. Jenson, B. Baker, and Q. Mo (2010), Microphysical and radiative properties of  
1018 tropical clouds investigated in TC4 and NAMMA, *J. Geophys. Res.*, this issue.

1019

1020 Lawson, R. P., D. O'Connor, P. Zmarzly, K. Weaver, B. A. Baker, Q. Mo, and H. Jonsson, 2006:  
1021 The 2D-S (Stereo) Probe: Design and Preliminary Tests of a New Airborne, High Speed,  
1022 High-Resolution Particle Imaging Probe. *J. of Atmos. and Oceanic Technol.*: Vol. 23., No. 11,  
1023 pp. 1462-1477.

1024

1025 Levelt, P. F., et al., The Ozone Monitoring Instrument, *IEEE Trans. on Geosci. and Rem. Sens.*,  
1026 44, 1093-1101, 2006.

1027

1028 McGill, M.J., D.L. Hlavka, W.D. Hart, J.D. Spinhirne, V.S. Scott, and B. Schmid, "The Cloud  
1029 Physics Lidar: Instrument description and initial measurement results", *Applied Optics*, 41,  
1030 pg. 3725-3734, June 2002.  
1031

1032 Minnis, P., L. Nguyen, R. Palikonda, J. K. Ayers, R. F. Arduini, F.-L. Chang, T. L. Chee, D. R.  
1033 Doelling, P. W. Heck, M. M. Khaiyer, M. L. Nordeen, W. L. Smith, Jr., D. A. Spangenberg, C.  
1034 R. Yost, P. Yang, and Y. Xie, (2010) Cloud properties determined from GOES and MODIS  
1035 data during TC4, *J. Geophys. Res.*, this issue.  
1036

1037 Morris, G.A., et. al. (2010), Observations of ozone production in a dissipating convective cell  
1038 during TC4, *J. Geophys. Res.*, this issue.  
1039

1040 Oltman, S.J., et. al., Ozone in the Pacific tropical troposphere from ozonesonde observations, *J.*  
1041 *Geophys. Res.*, 106, 32503-32526, 2001.  
1042

1043 Pearson R.W. and D.H. Stedman (1980), Instrumentation for fast response ozone  
1044 measurements from aircraft, *Atmos Tech*, 12.  
1045

1046 Pfister, L., H.B. Selkirk, D. O'C. Starr, P.A. Newman, and K.H. Rosenlof (2010), A meteorological  
1047 overview of the TC4 mission, *J. Geophys. Res.*, this issue.  
1048

1049 Pickering, K. E., R. R. Dickerson, G. J. Huffman, J. F. Boatman and A. Schanot, (1988), Trace  
1050 Gas Transport in the Vicinity of Frontal Convective Clouds, *J. Geophys. Res.*, **93**, 759-773.  
1051

1052 Pickering, K. E., A. M. Thompson, Y. Wang, W.-K. Tao, D. P. McNamara, V.W.J.H. Kirchoff, B.G.  
1053 Heikes, G. W. Sachse, J. D. Bradshaw, G. L. Gregory, D. R. Blake, (1996), Convective  
1054 transport of biomass burning emissions over Brazil during TRACE-A, *J. Geophys. Res.*, 101,  
1055 D19, doi:10.1029/96JD00346.

1056

1057 Ridley, B. A., M. A. Avery, J. V. Plant, S. A. Vay, D. D. Montzka, A. J. Weinheimer, D. J. Knapp,  
1058 J. E. Dye, E. C. Richard, (2006), Sampling of Chemical Constituents in Electrically Active  
1059 Convective Systems: Results and Cautions, *J. Atmos. Chem.*, 10.1007/s10874-005-9007-5.

1060

1061 Sachse, G., G. Hill, L. Wade, and M. Perry (1987), Fast-Response, High-Precision Carbon  
1062 Monoxide Sensor Using a Tunable Diode Laser Absorption Technique, *J. Geophys. Res.*,  
1063 92(D2), 2071-2081.

1064

1065 Scheuer, E., J.E. Dibb, C. Twohy, D.C. Rogers, A.J. Heymsfield, and A. Bansommer (2010),  
1066 Evidence of nitric acid uptake in warm cirrus clouds during the NASA TC4 campaign, *J.*  
1067 *Geophys. Res.*, this issue.

1068

1069 Schoeberl, M. R., J. R. Ziemke, B. Bojkov, et al. (2007), A trajectory-based estimate of the  
1070 tropospheric ozone column using the residual method, *J. Geophys. Res.*, 112, D24S49,  
1071 doi:10.1029/2007JD008773.

1072

1073 Scott, S.G., T.P. Bui, K. R. Chan, and S. W. Bowen (1990), The meteorological measurement  
1074 system on the NASA ER-2 aircraft, *J. Atmos. Ocean. Tech.*, 7, 525-540.

1075

1076 Selkirk, H.B., H Vomel, J.Valverde, and L. Pfister (2010), The detailed structure of the tropical  
1077 upper atmosphere as revealed by balloonsonde observations of water vapor, ozone,  
1078 temperature and winds during the NASA TCSP and TC4 campaigns, *J. Geophys. Res.*, this  
1079 issue.

1080

1081 Solomon, S., D.W.J. Thompson, R.W. Portmann, S.J. Oltmans, and A.M. Thompson (2005), On  
1082 the distribution and variability of ozone in the tropical upper troposphere: Implications for

1083 tropical deep convection and chemical-dynamical coupling, *Geophys. Res. Lett.*, 32, L23813,  
1084 doi:10.1029/2005GL024323.

1085

1086 Spencer, K.M., D. C. McCabe, J. D. Crouse, J. R. Olson, J. H. Crawford, A. J. Weinheimer, D. J.  
1087 Knapp, D. D. Montzka, C. A. Cantrell, R. S. Hornbrook, R. L. Mauldin III, and P. O. Wennberg  
1088 (2009), Inferring ozone production in an urban atmosphere using measurements of  
1089 peroxyacetic acid, *Atmos. Chem. Phys.*, 9, 3697-3707.

1090

1091 Thompson, A.M. et. al. (2010), Convective and wave signatures in ozone profiles over the  
1092 equatorial Americas: Views from TC4 (2007) and SHADOZ, *J. Geophys. Res.*, this issue.

1093

1094 Thompson, A.M., J.E. Yorks, S.K. Miller, J.C. Witte, K.M. Dougherty, G.A. Morris, D.  
1095 Baumgardner, L. Ladibno, and B. Rappenglueck, Tropospheric ozone sources and wave  
1096 activity over Mexico City and Houston during Milagro/Intercontinental Transport Experiment  
1097 (INTEXB) Ozonesonde Network Study, 2006 (IONS-06), *Atmos. Chem. Phys.*, 8, 5113-5125,  
1098 2008.

1099

1100 Toon, O.B., D. O'C. Starr, E. Jensen, P. Newman, S. Platnik, M. Schoeberl, P. Wennberg, S.  
1101 Wofsy, M. Kurylo, H. Maring, K. Jucks, M. Craig, M. Vasquez, et. al., Planning and overview  
1102 of the Tropical Composition, Cloud and Climate Coupling Experiment, *J. Geophys. Res.*, this  
1103 issue.

1104

1105 Twohy, C.H., Schanot, A.J. and W.A. Cooper, 1997: Measurement of condensed water content in  
1106 liquid and ice clouds using an airborne counterflow virtual impactor, *J. Atmos. Oceanic  
1107 Technol.*, **14**, 197-202.

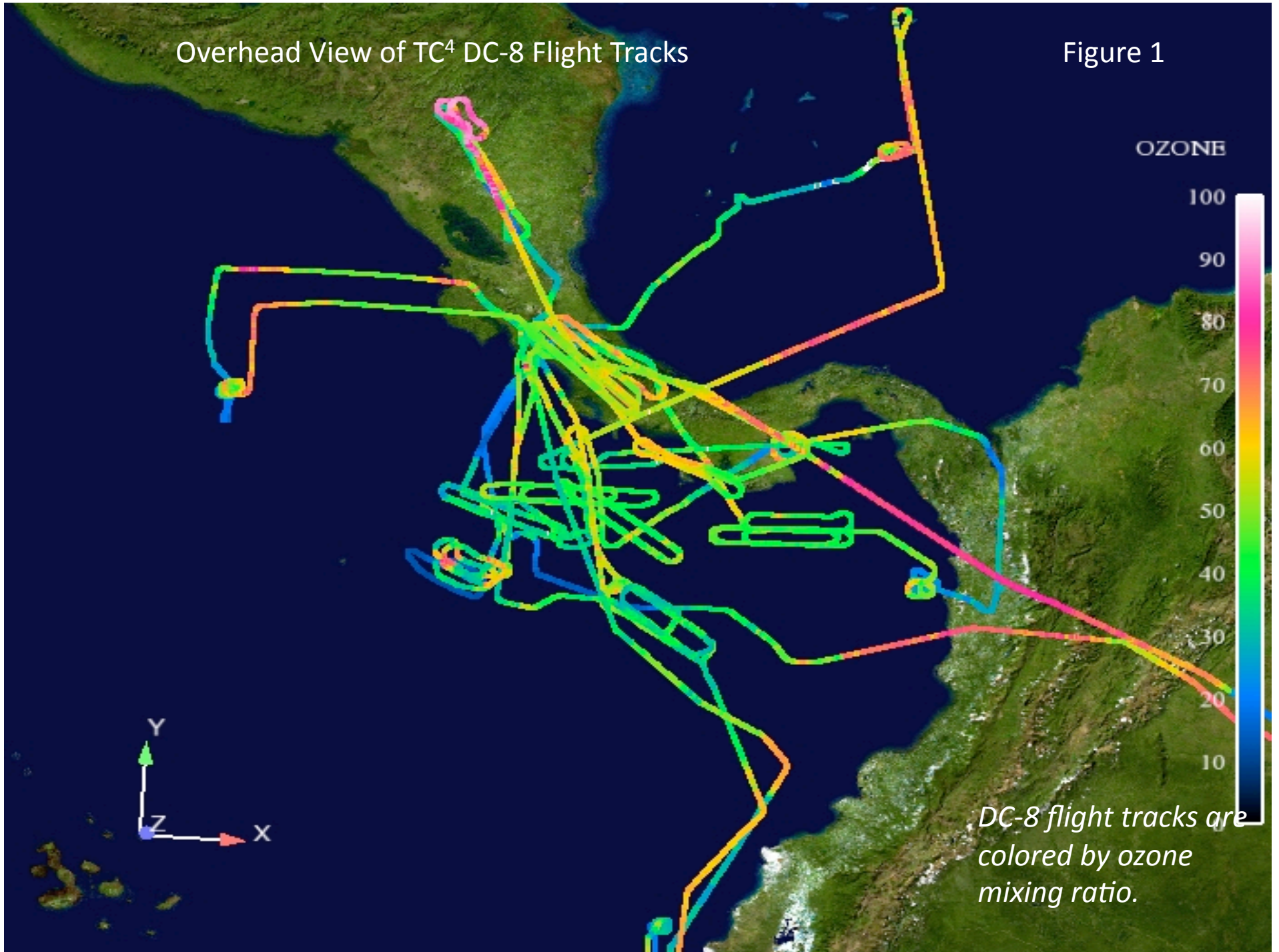
1108

1109 Vasilkov, A. P., J. Joiner, R. Spurr, P.K. Bhartia, P. F. Levelt, and G. Stephens, Evaluation of the  
1110 OMI cloud pressures derived from rotational-Raman scattering by comparisons with satellite

1111 data and radiative transfer simulations, *J. Geophys. Res.*, **113**, D15S19,  
1112 doi:10.1029/2007JD008689.  
1113  
1114 Winker, D. M., W. H. Hunt, and M. J. McGill, (2007), Initial performance assessment of CALIOP,  
1115 *Geophys. Res. Lett.*, 34, L19803, doi:10.1029/2007GL030135.  
1116  
1117 Ziemke, J. R., J. Joiner, S. Chandra, P. K. Bhartia, A. Vasilkov, D. P. Haffner, K. Yang, M. R.  
1118 Schoeberl, L. Froidevaux, and P. F. Levelt (2009), Ozone mixing ratios inside tropical deep  
1119 convective clouds from OMI satellite measurements, *Atm. Chem. Phys.*, 9, 573-583.  
1120  
1121 Ziemke, J. R., S. Chandra, and P. K. Bhartia (2001), "Cloud slicing": A new technique to derive  
1122 upper tropospheric ozone from satellite measurements, *J. Geophys. Res.*, 106, 9853-9867.  
1123  
1124  
1125

Overhead View of TC<sup>4</sup> DC-8 Flight Tracks

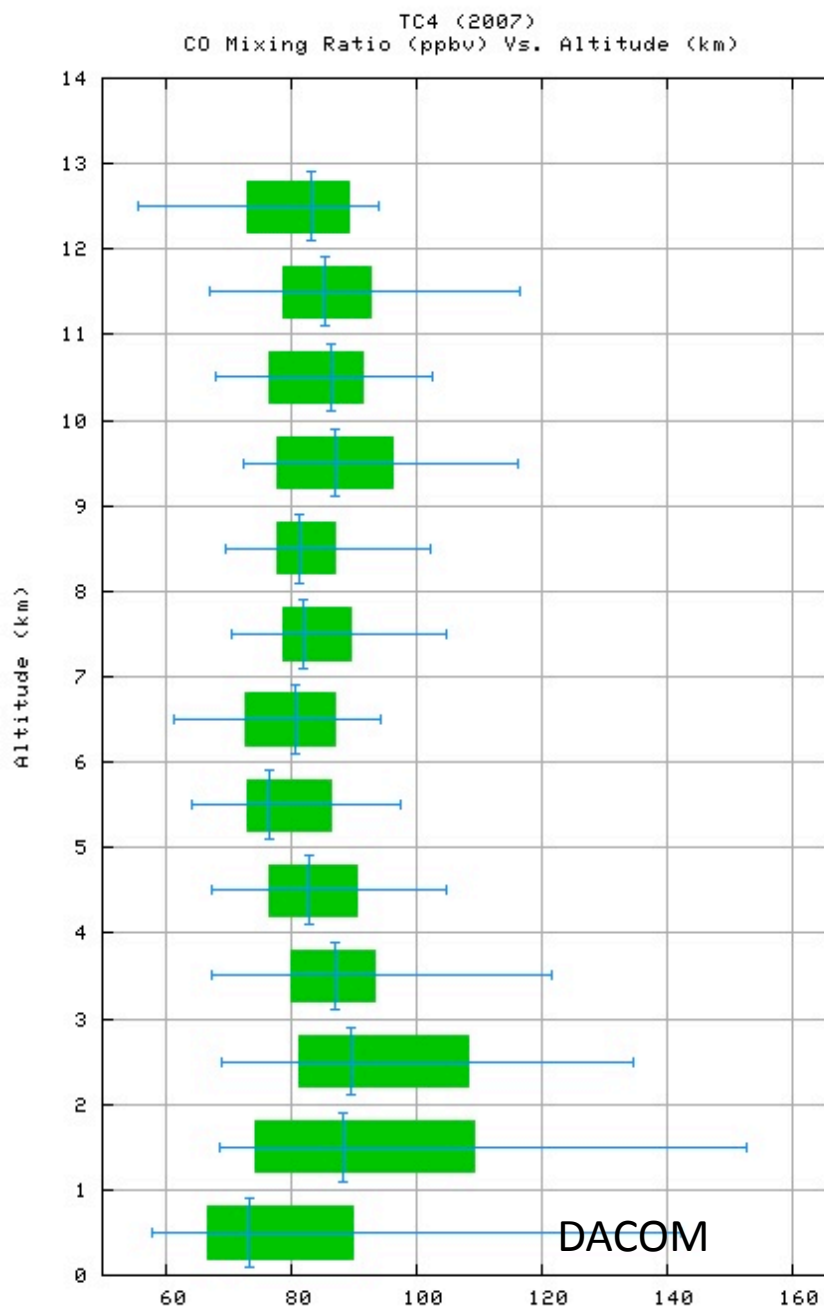
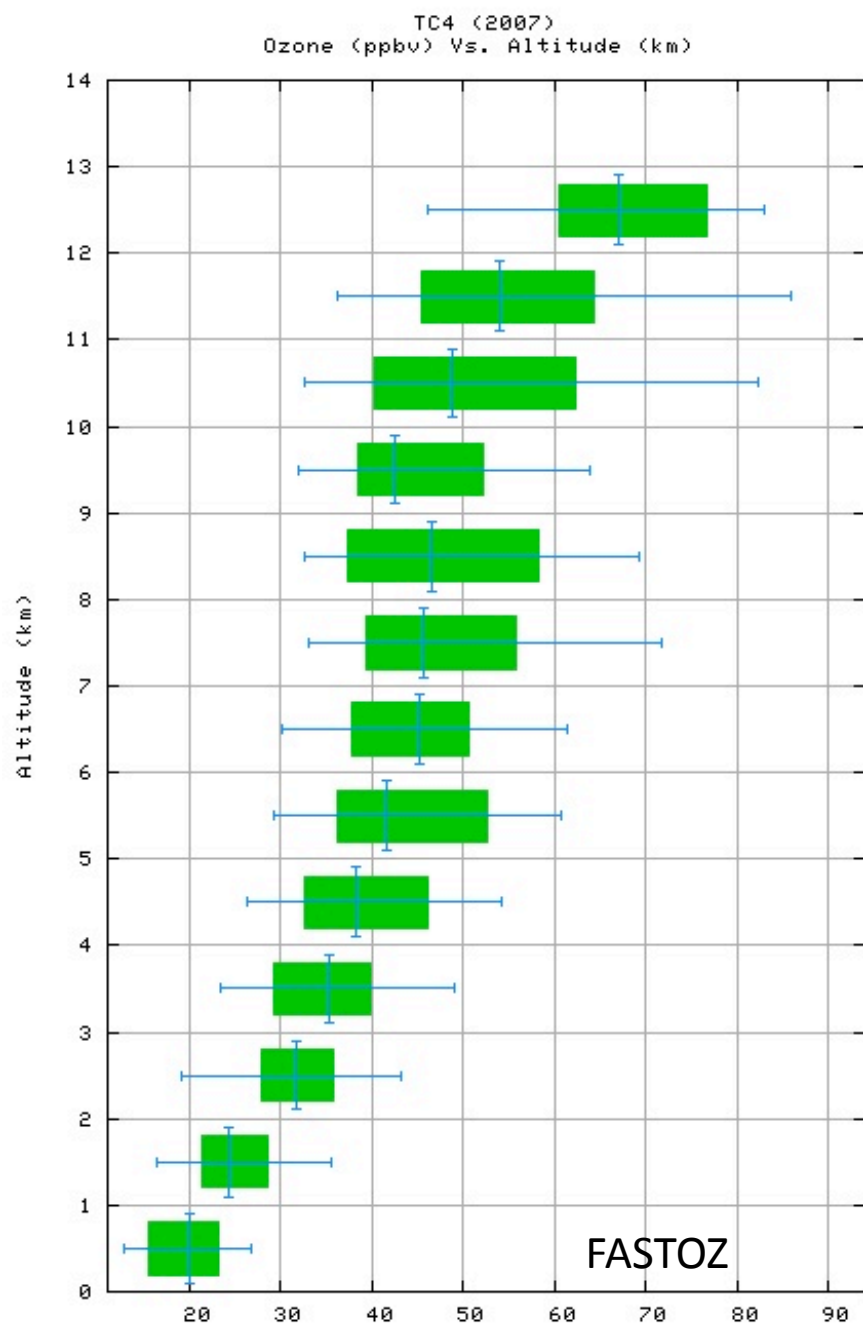
Figure 1



*DC-8 flight tracks are colored by ozone mixing ratio.*

TC<sup>4</sup> O<sub>3</sub> and CO Median Profiles, 7S-17N, 270-290W

Figure 2



FASTOZ Median Ozone Profiles, 7S-17N  
Pacific Missions

Figure 3

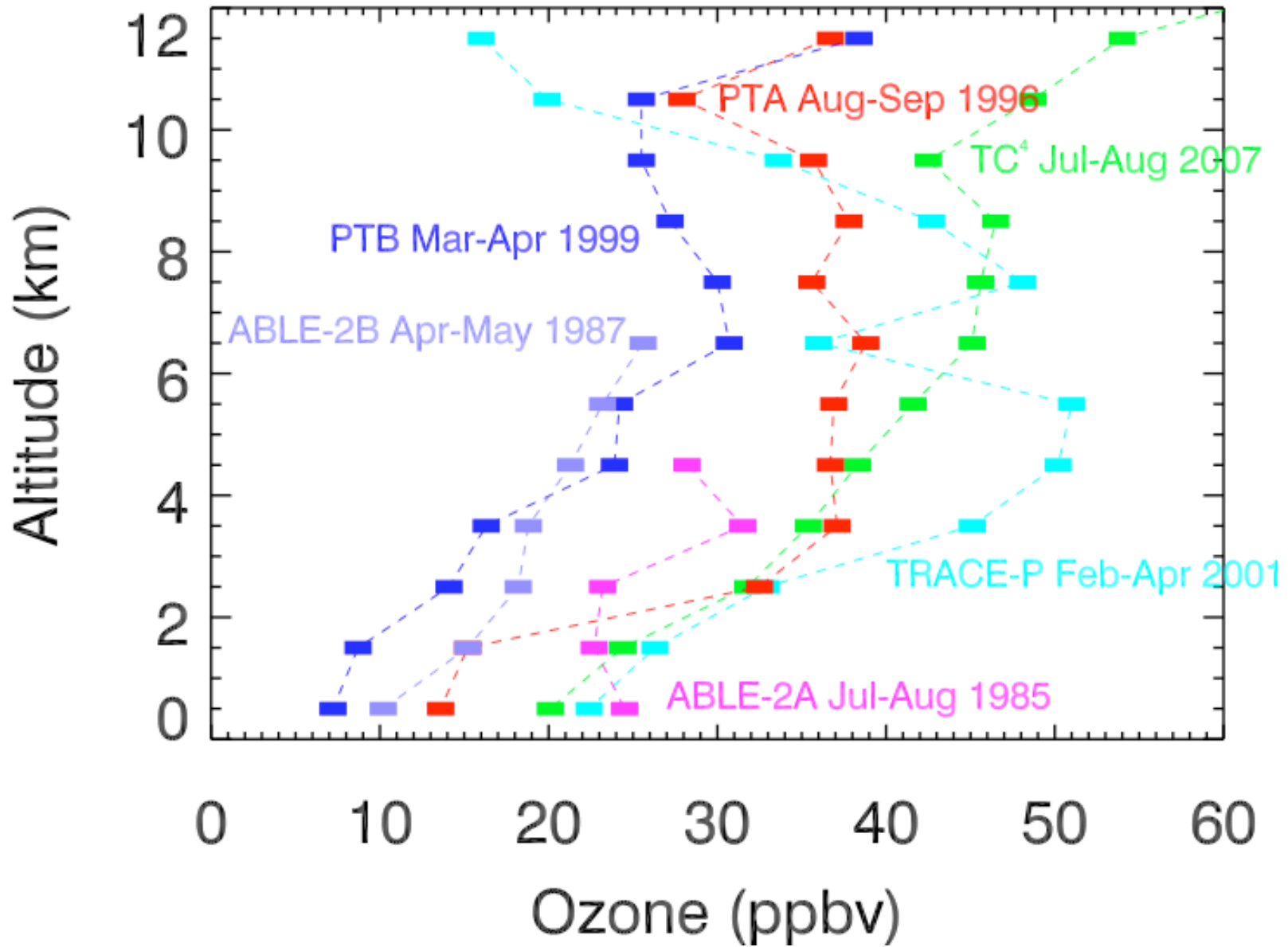
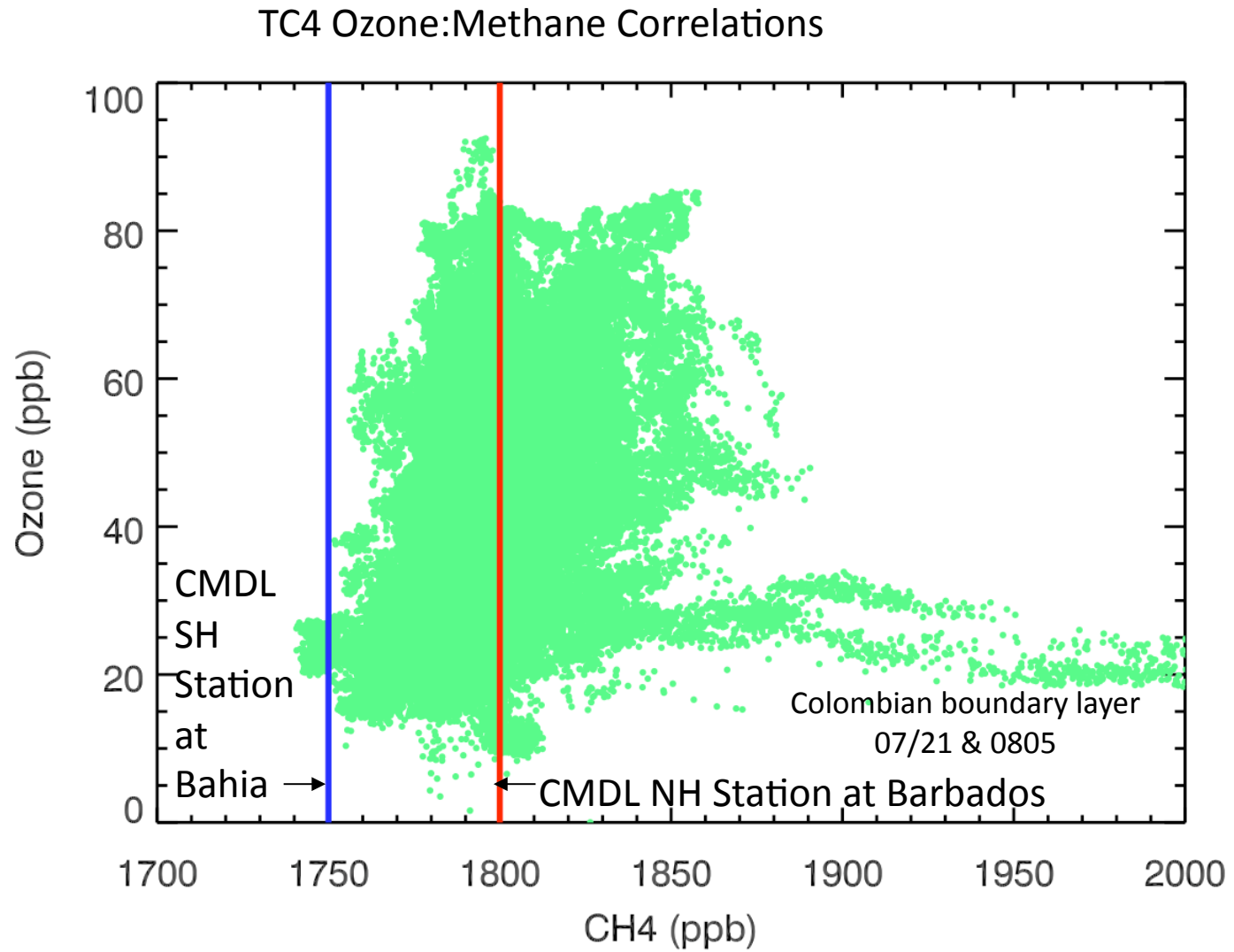


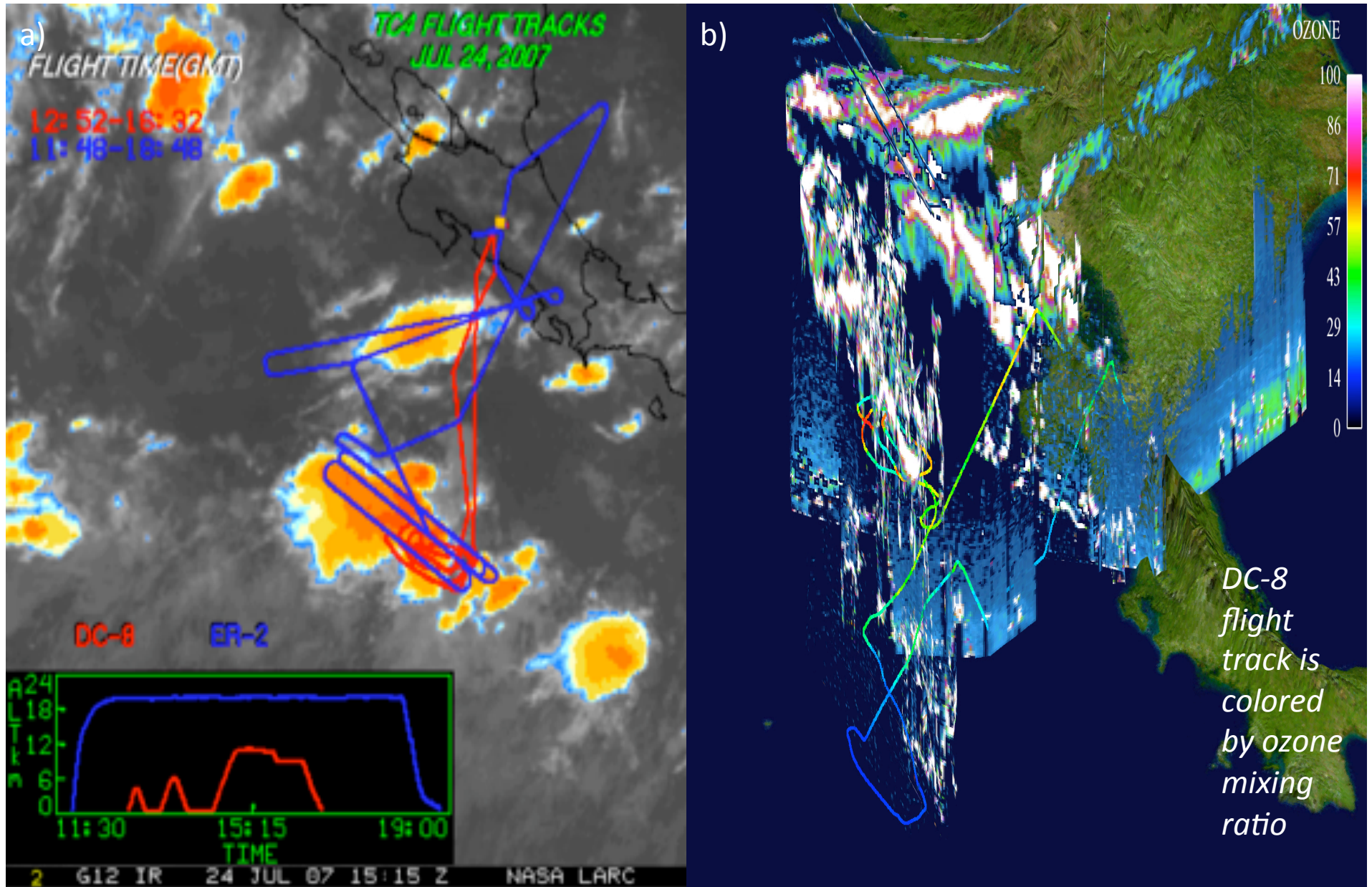
Figure 4



NOAA/CMDL methane data: K. A. Masarie and E. Dlugokencky

July 24, 2007 DC-8 and ER-2 Sampling of Rapidly Developing Convection

Figure 5



Strong Convection on July 24, 2007  
During TC4

Figure 6

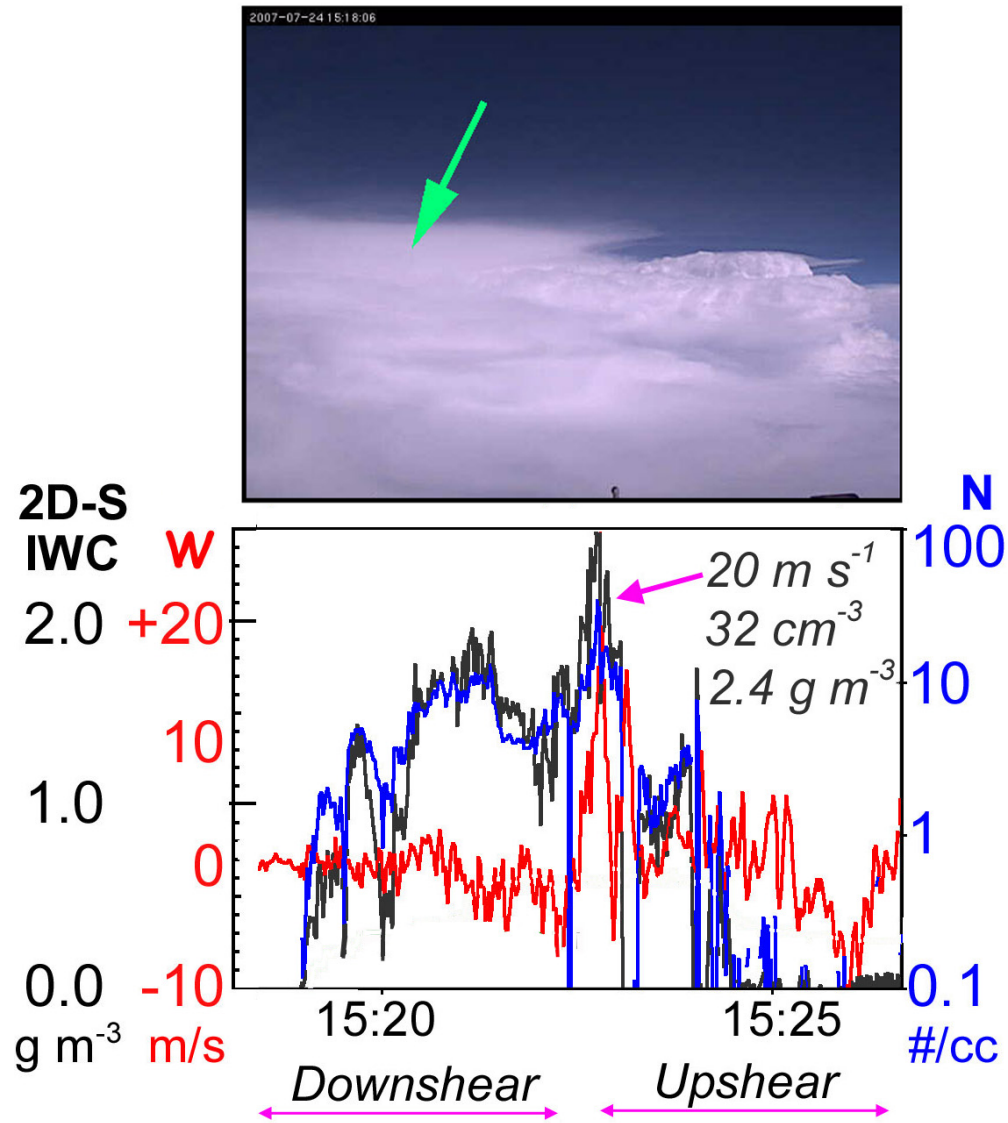


Figure 7

Upper Tropospheric Tracer Time Series  
in Developing Convection

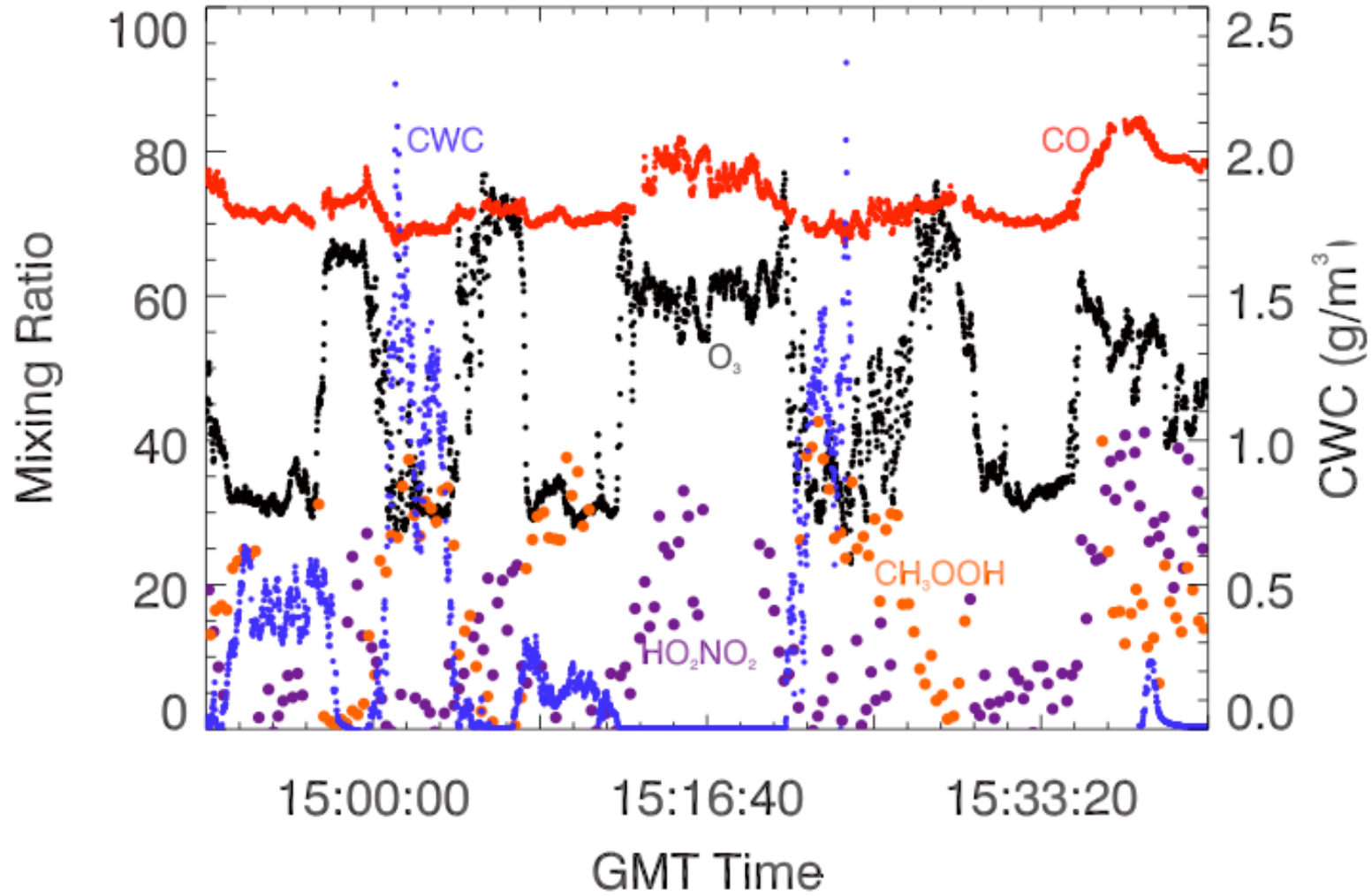


Figure 8

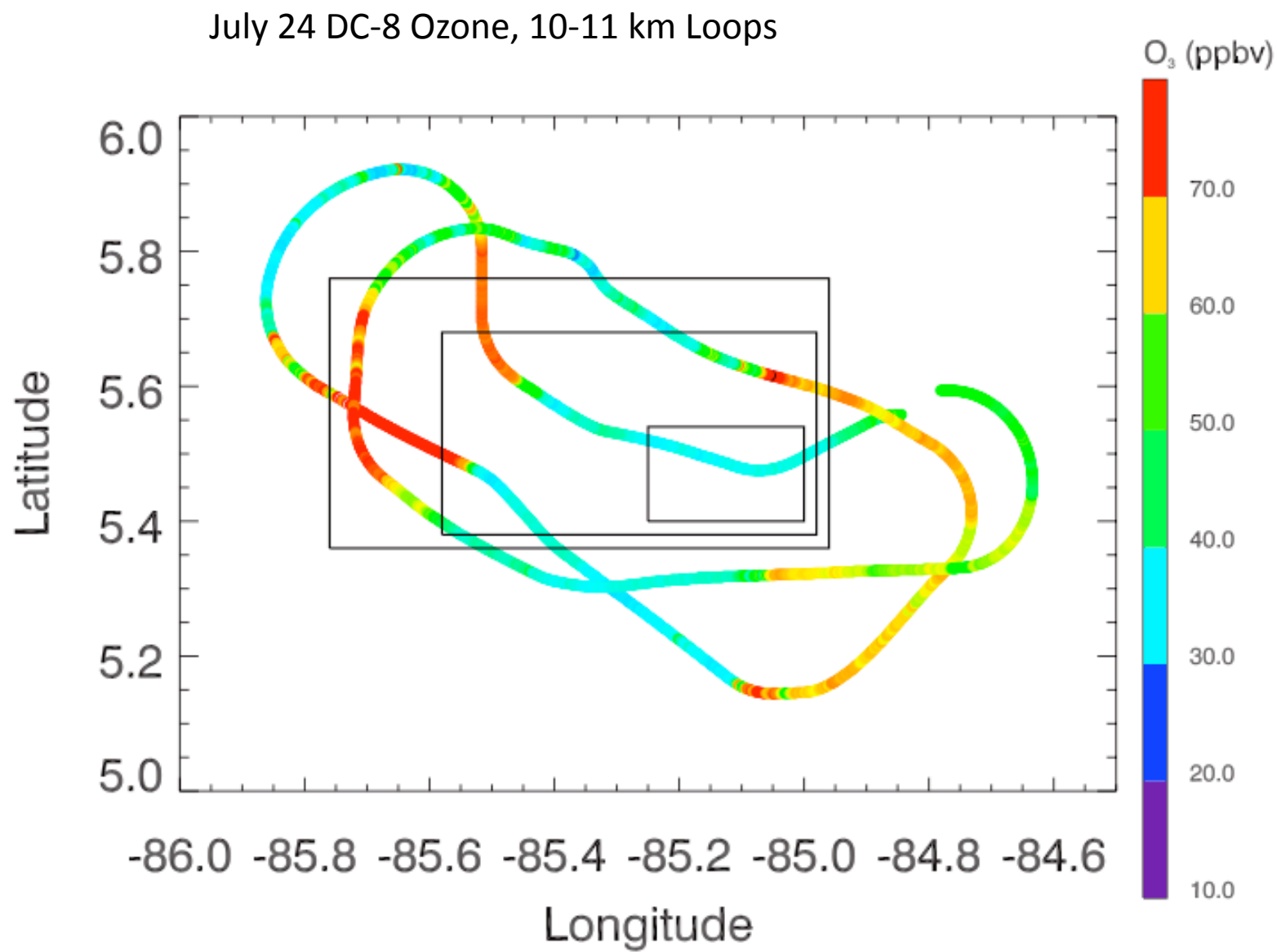
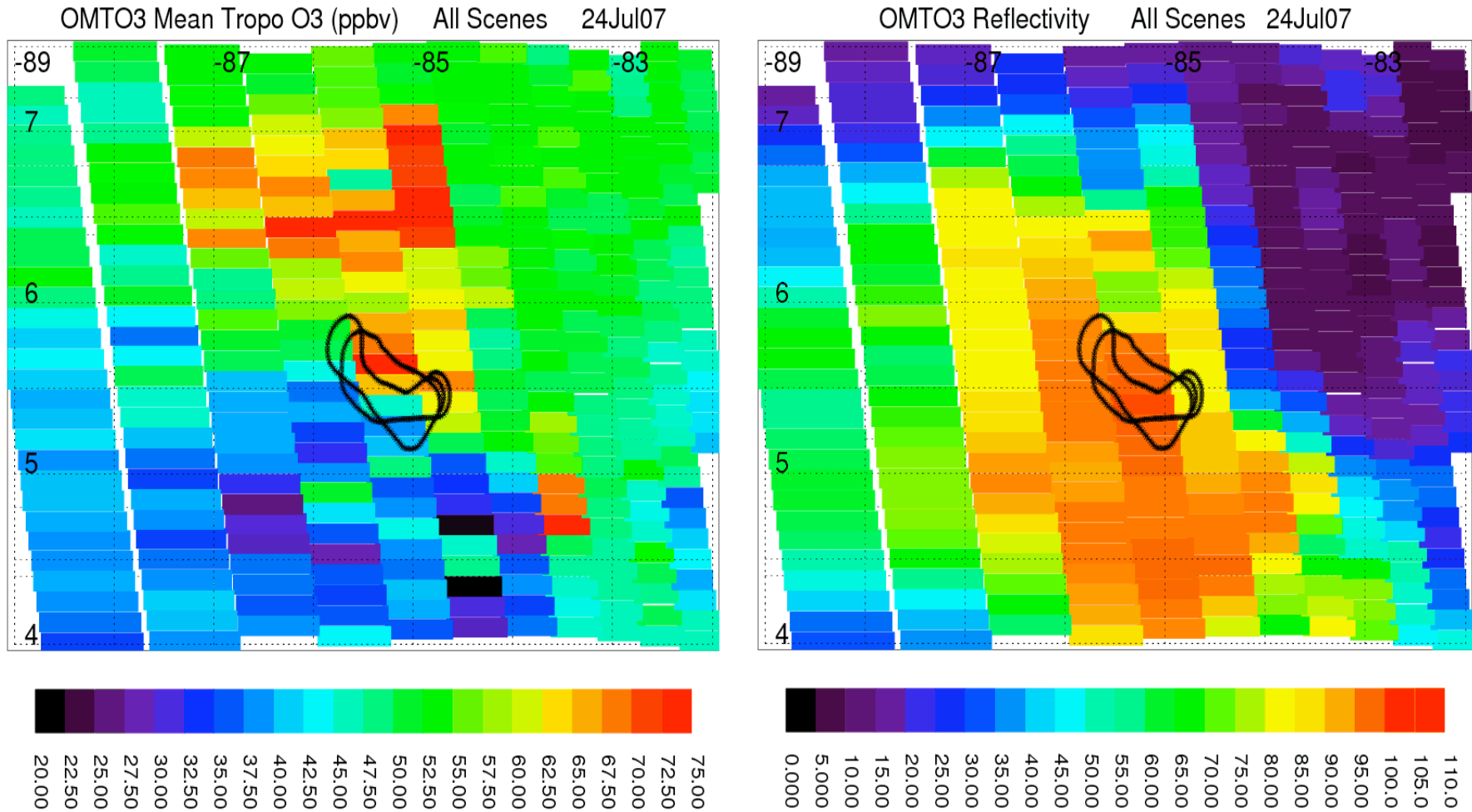


Figure 9

# OMI Tropospheric Ozone Mean Volume Mixing Ratio (left) and Reflectivity (right) for 24 July 2007



(Black curves: Flight Path for Air Pressure < 300 hPa)

Figure 10

# August 5 Close-Up of Convective Outflow

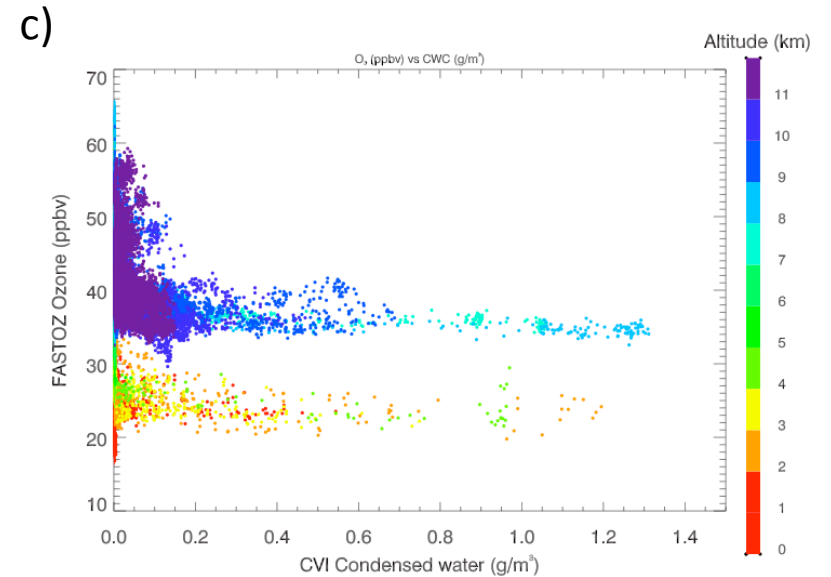
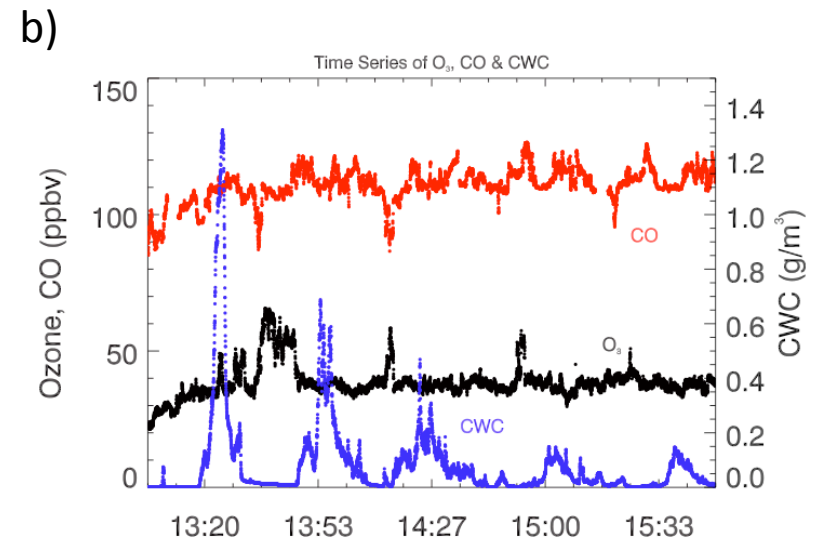
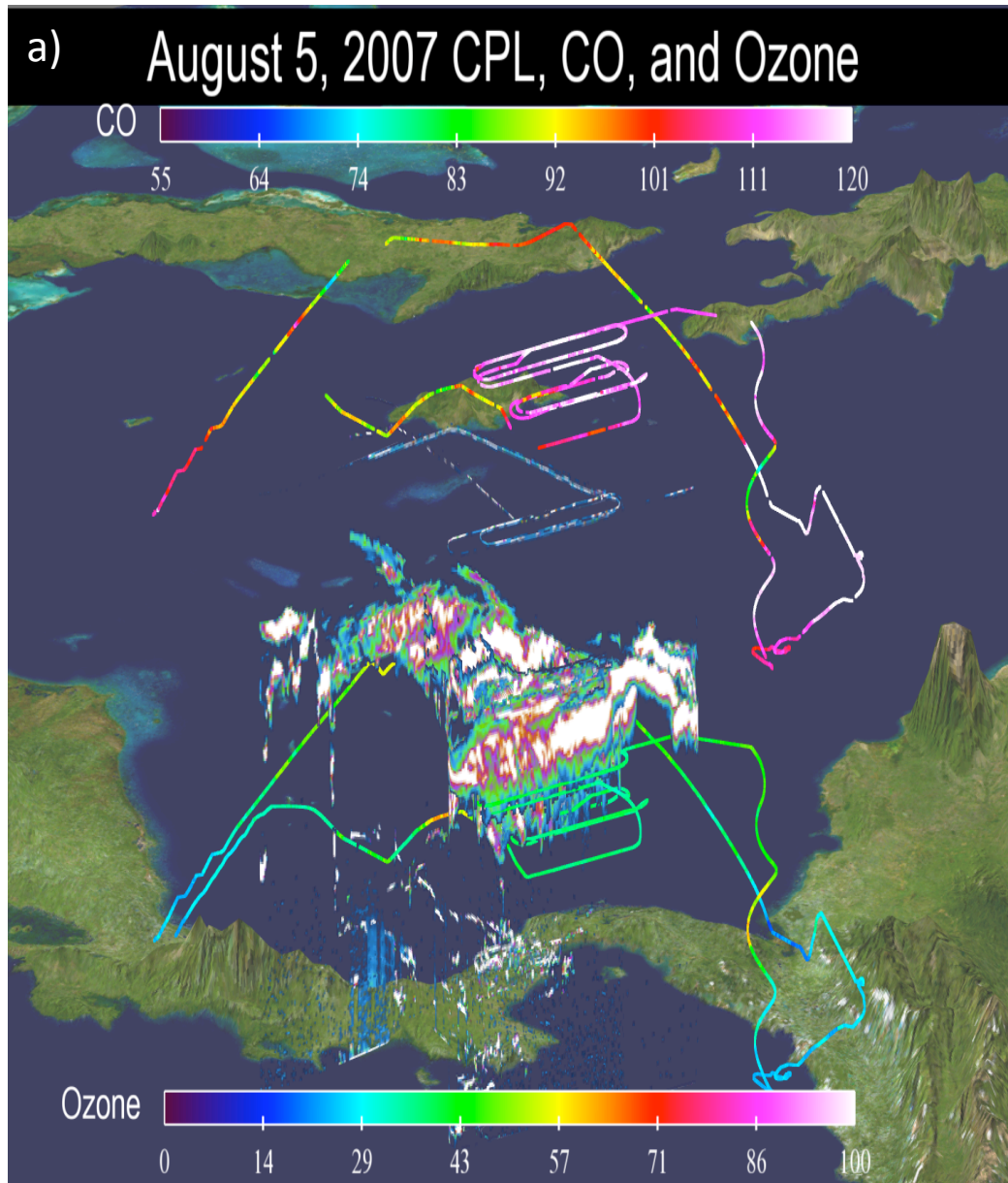


Figure 11

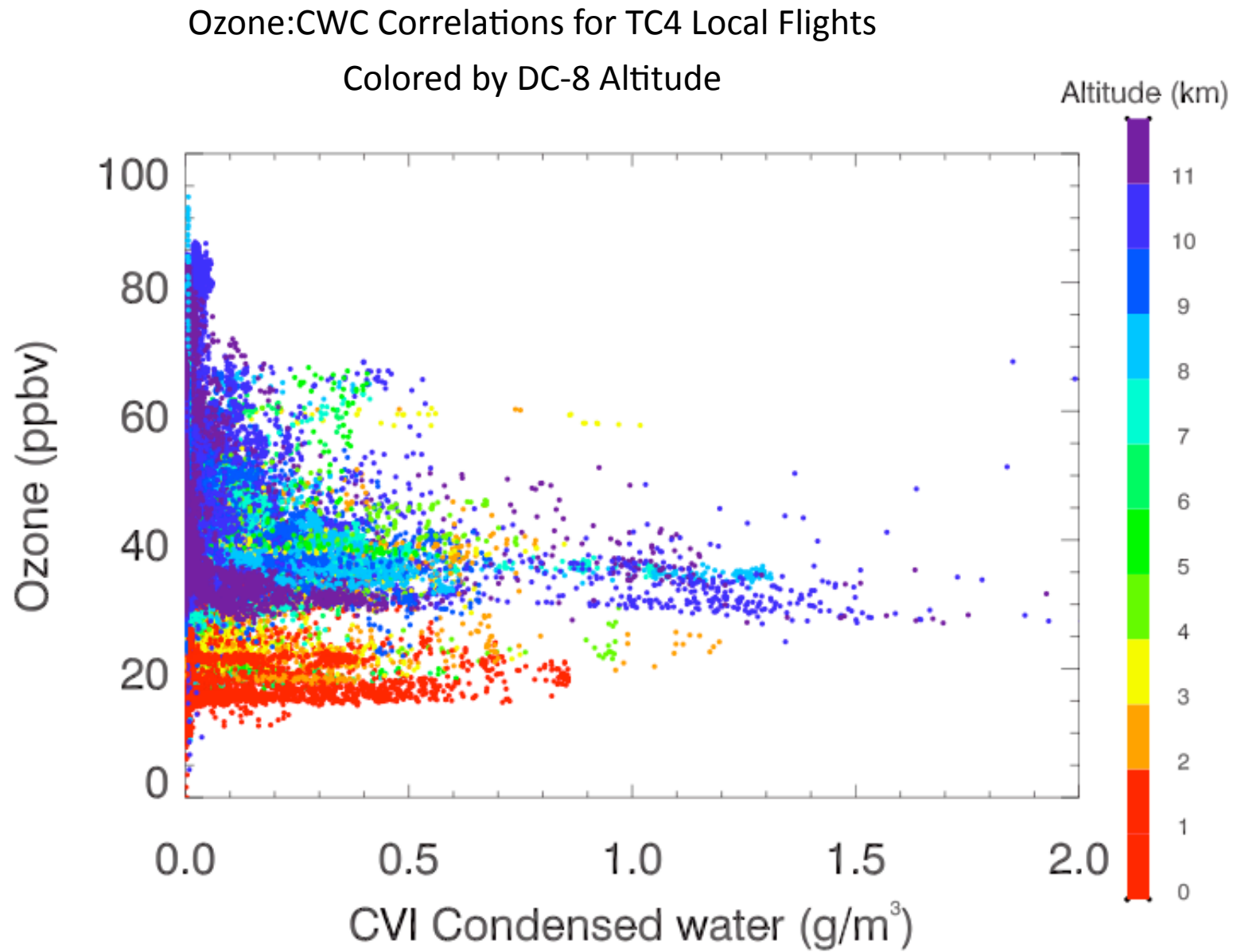


Figure 12

Probability Histograms of Ozone and Carbon Monoxide  
In Clouds and Outside of Clouds

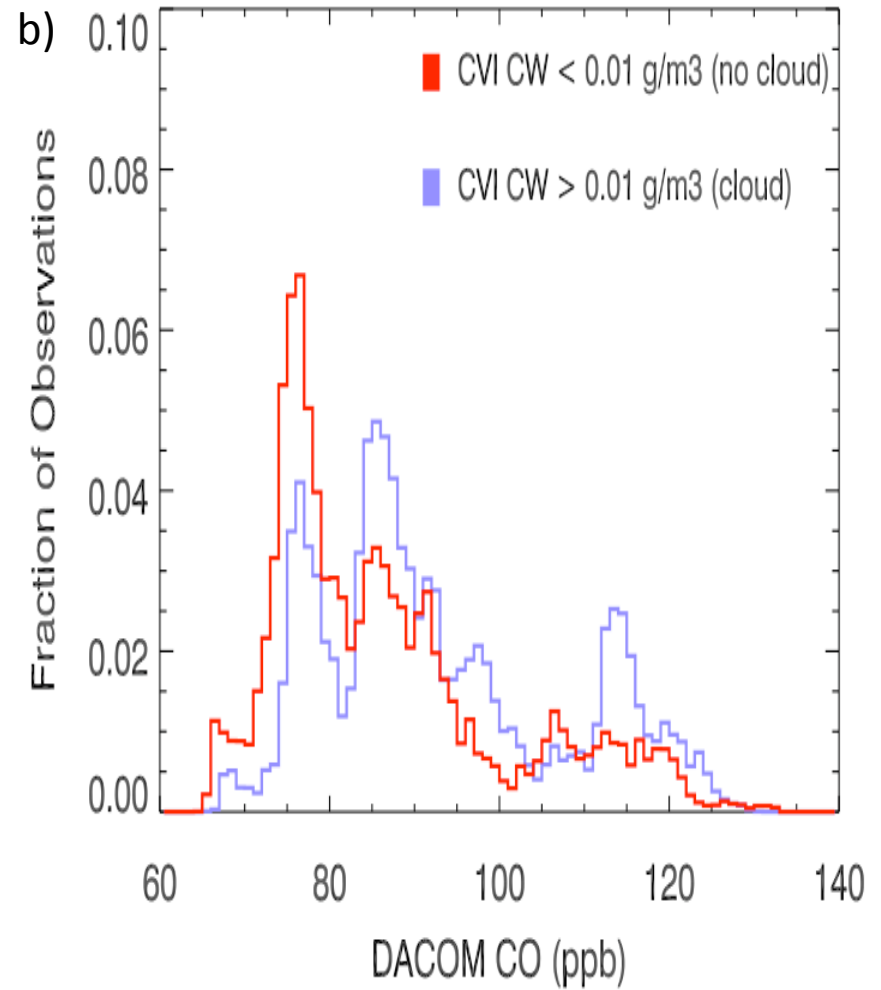
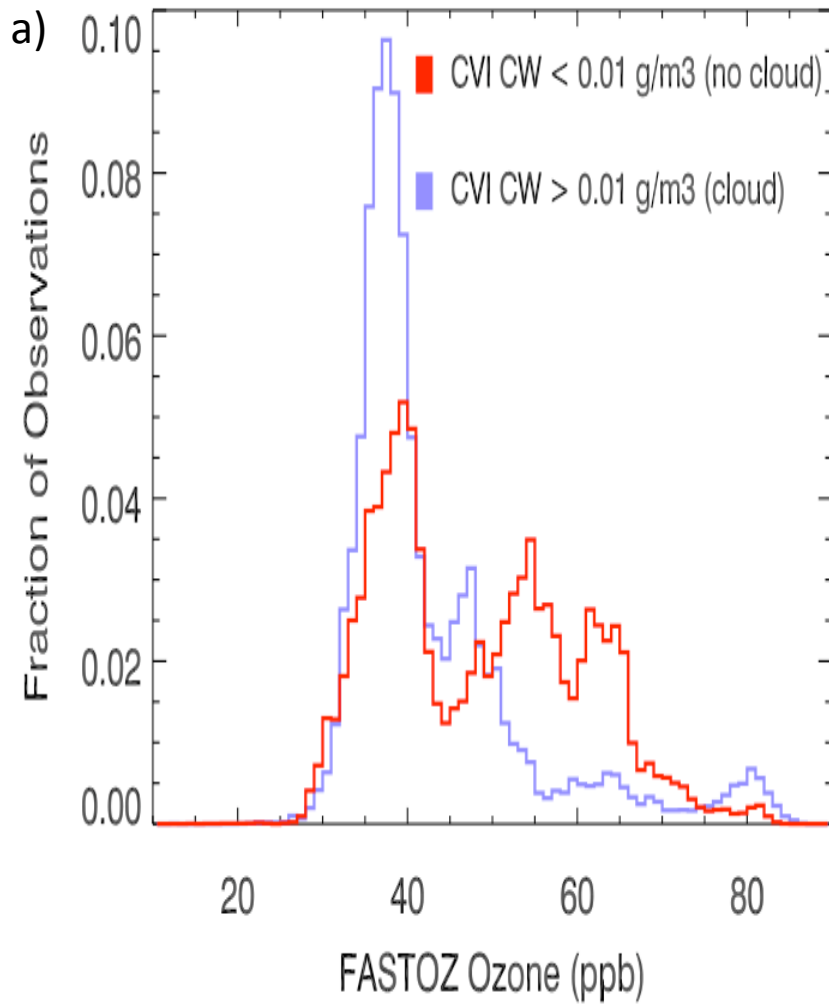
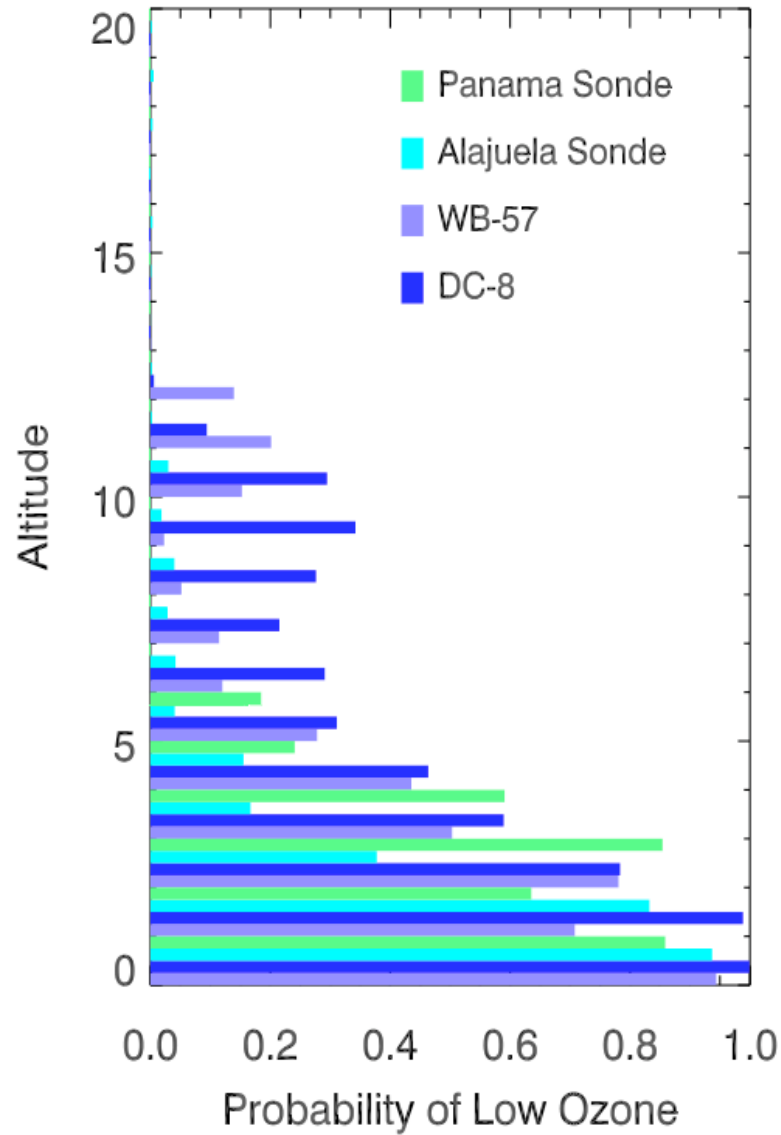


Figure 13

a) Probability of  $O_3 < 44$  ppbv



b) Probability of  $O_3 < 28$  ppbv

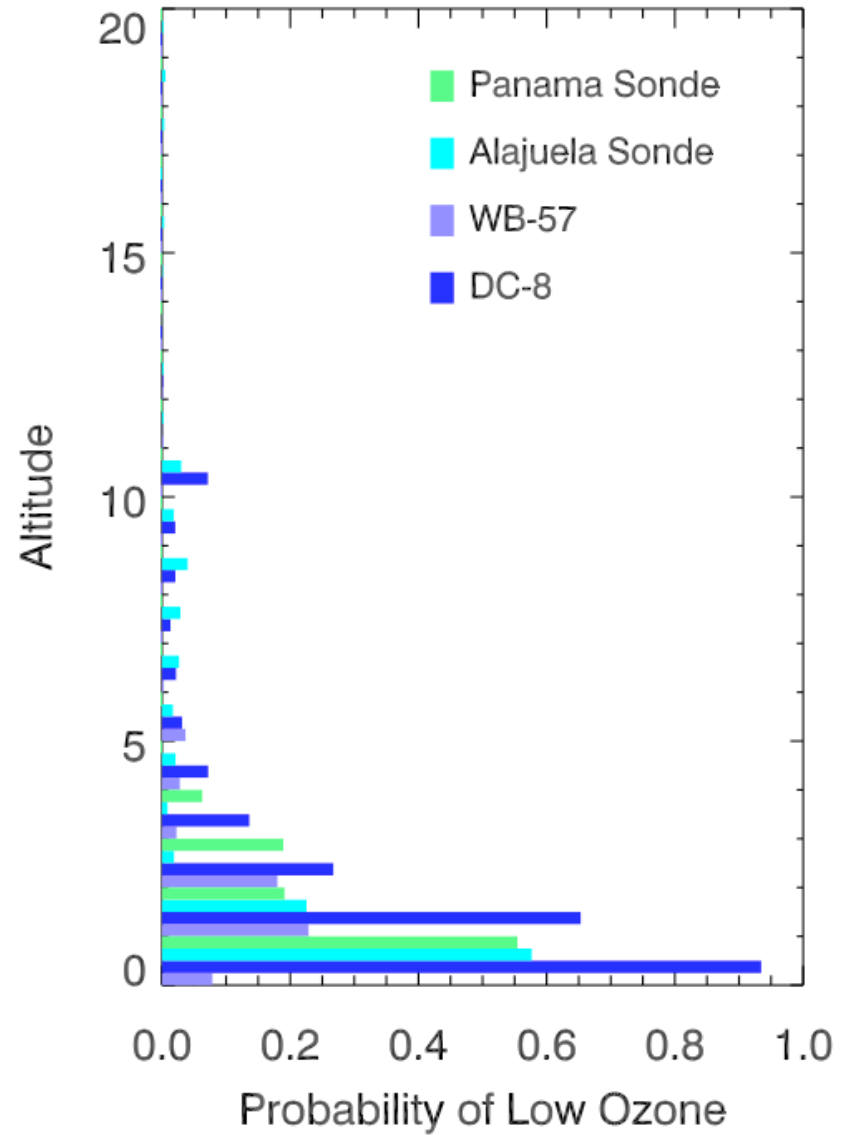


Figure 14

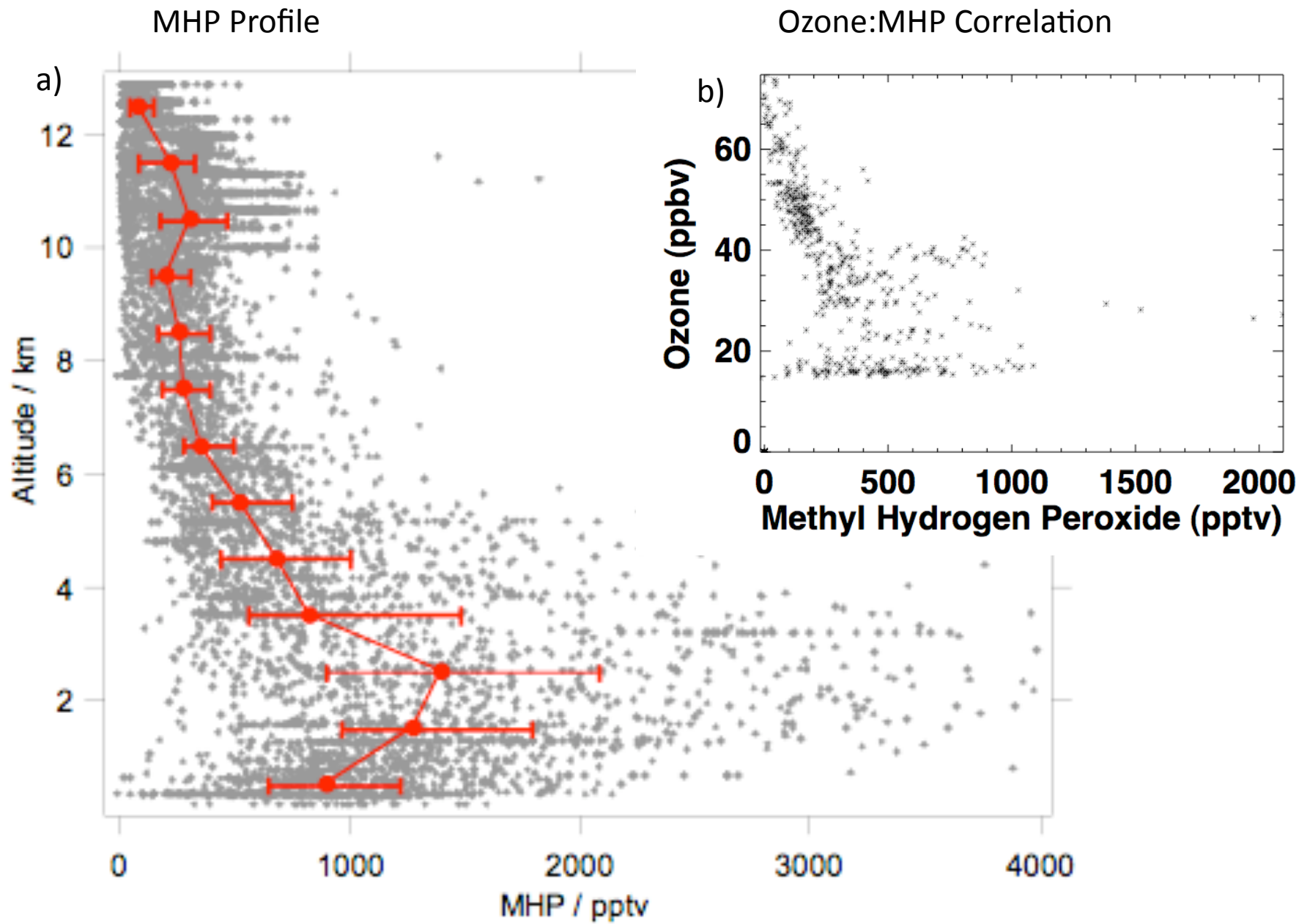
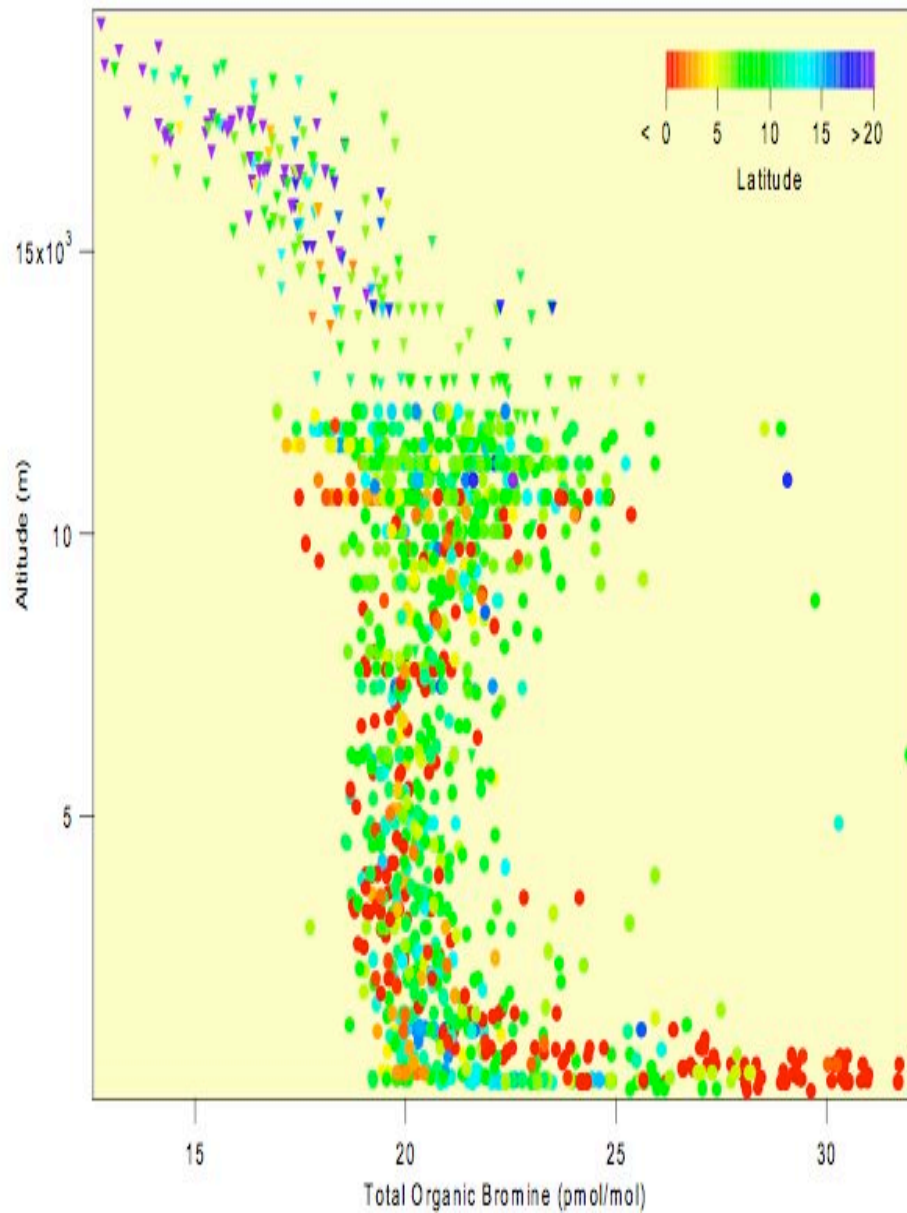


Figure 15

a) Total Organic Bromine Vertical Profile During TC4



b) Aggregate Calcium Profile

